May 13th, 2021

Field evidence for disequilibrium dynamics in preserved fluvial cross-strata: A record of discharge variability or morphodynamic hierarchy?

Sinéad J. Lyster[1], Alexander C. Whittaker[1], Elizabeth A. Hajek[2] and Vamsi Ganti[3,4]*

[1]Department of Earth Science and Engineering, Imperial College London, London, UK.
[2]Department of Geosciences, The Pennsylvania State University, Pennsylvania, USA.
[3]Department of Geography, University of California Santa Barbara, California, USA.
[4]Department of Earth Science, University of California Santa Barbara, California, USA.
**s.lyster17@imperial.ac.uk*

Abstract

Bedforms preserved in the rock record can provide detailed information on the morphologies and hydrodynamics of ancient fluvial systems on Earth and other planets. Existing process–product relations for bedform preservation assume that fluvial cross strata reflect conditions under which bedforms were equilibrated with the prevailing flow, i.e., steady-state conditions. However, recent theoretical and experimental observations indicate that enhanced bedform preservation can occur in non-steady state, or disequilibrium, conditions, and it is currently unclear how prevalent disequilibrium dynamics are in preserved field-scale fluvial strata. Here we explore whether steady-state assumptions are appropriate for ancient fluvial systems by evaluating the nature of bedform preservation in well studied fluvial deposits of three Late Cretaceous (Turonian and Campanian) geologic formations in central Utah, USA: the Blackhawk Formation, Castlegate Sandstone, and Ferron Sandstone. In the field, we made systematic measurements of cross-set heights to quantify the extent to which preserved cross-sets reflect bedform preservation in steady-state conditions. Across the three formations, unanimously low coefficients of variation in preserved cross-set heights of 0.25–0.5 are inconsistent with bedform preservation in steady-state conditions, and instead point to fluvial systems in which enhanced preservation of bedforms occurred in disequilibrium conditions.

Enhanced bedform preservation in fluvial strata can be explained by two independent hypotheses: the effect of flashy flood hydrographs on bedform preservation (flood hypothesis) or bedform preservation in the presence of a morphodynamic hierarchy (hierarchy hypothesis). We estimated bedform turnover timescales to quantitatively assess these competing hypotheses and contextualize their implications. Under the flood hypothesis, field measurements are consistent with enhanced bedform preservation driven by flashy flood hydrographs with flood durations ranging on the order of hours to a few days, which are consistent with perennial fluvial systems subject to heavy rains and tropical storms. Alternatively, under the hierarchy hypothesis, field measurements are consistent with bedform climb angles that range from 10^{-2} to 10^{-1}, reflecting rapid bar migration. Our work provides a novel way of investigating fluvial discharge variability in the geologic past, and we

outline the potential next steps to disentangle the relative controls of flood variability and morphodynamic hierarchy in controlling bedform preservation in ancient fluvial systems.

Keywords

Fluvial systems; Bedforms; Cross strata; Hydrodynamics; Morphodynamics; Discharge variability

1. Introduction

Quantitative reconstructions of palaeohydraulics from fluvial stratigraphy complement qualitative observations of sedimentary facies to build more complete pictures of palaeo-landscapes on Earth and other planets. In fluvial strata, preserved bedforms are crucial to these reconstructions. Bedforms are readily formed on riverbeds across a range of grain sizes (e.g., Carling, 1999; Best, 2005) and their evolution generates cross-stratification — the resultant cross strata are a fundamental building block of alluvium on planetary surfaces (e.g., Allen, 1982; Edgar et al., 2018). Cross strata provide a window to formative conditions in ancient fluvial systems and are routinely used to reconstruct morphologies and hydrodynamics (Holbrook & Wanas, 2014; Ganti et al., 2019; Wang et al., 2020; Lyster et al., 2021); for instance, measurements of cross-set heights provide a mechanism to estimate the sizes of dunes active on ancient river beds and, therefore, palaeoflow depths (Leclair & Bridge, 2001; Bradley & Venditti, 2017). Moreover, bedform kinematics and geometries respond to spatial and temporal changes in flow and sediment transport conditions (e.g., Ten Brinke et al., 1999; Martin & Jerolmack, 2013; Wu et al., 2020), and recent research has highlighted that these changes may be recorded in preserved cross-set geometries (Leary & Ganti, 2020). If we can use cross stratal geometries to extract information about water and sediment discharge variability, this would significantly improve our understanding of ancient fluvial systems, including river response to climatic perturbation (e.g., Foreman et al., 2012; Colombera et al., 2017). However, a crucial outstanding challenge of this work involves adapting engineering-scale insights, which are typically founded in precisely defined boundary conditions (and which underpin palaeohydraulic reconstructions), to geological scales over which more variability in environmental conditions is typically assumed due to issues of time-averaging and temporal incompleteness in the rock record (e.g., Romans et al., 2016; Straub et al., 2020).

Process–product relationships between bedform evolution and cross stratal geometries have primarily been studied using small-scale physical experiments and numerical models (Paola & Borgman, 1991; Bridge, 1997; Leclair, 2002; Jerolmack & Mohrig, 2005; Ganti et al., 2013; Wu et al., 2020). Existing models that relate cross-set heights to original bedform heights rely on the assumption that the formative train of bedforms evolved in steady-state conditions under no-net aggradation or with a small ($<10^{-2}$) bedform climb angle (Paola & Borgman, 1991; Jerolmack & Mohrig, 2005). For a range of these formative conditions, theory, numerical models and experimental observations suggest the bedform preservation ratio — defined as the ratio of the average preserved cross-set heights and the average original bedform heights — is a near-constant value of 0.3 (Paola & Borgman, 1991; Leclair & Bridge, 2001; Leclair, 2002; Jerolmack & Mohrig, 2005). Further, these models predict that the coefficient of variation, *CV*, of cross-set heights has a constant value of 0.88 (Paola & Borgman, 1991; Leclair & Bridge, 2001; Leclair, 2002; Jerolmack & Mohrig, 2005), with Bridge (1997) suggesting that the steady-state model for bedform preservation can be applied so long as the *CV* of cross-set heights is bounded by 0.88±0.30. While these insights have primarily been supported by numerical and experimental studies under steady-state conditions (e.g., Leclair, 2002; Ganti et al., 2013; Leary & Ganti, 2020), they are widely applied in field-scale palaeohydrological studies (e.g., Holbrook & Wanas, 2014; Ganti et al., 2019; Wang et al., 2020; Lyster et al., 2021).

However, steady-state conditions, strictly defined, are commonly violated in natural systems when discharge is variable (e.g., Fielding et al., 2018; Ghinassi et al., 2018; Herbert et al., 2020), or under relatively constant flow conditions in which spontaneously developed features, such as bars, establish complex and locally variable flow conditions that change as bars shift and channels migrate (Reesink et al., 2015; Chamberlin & Hajek, 2019; Ganti et al., 2020; Wysocki & Hajek, 2021). These non-steady, or disequilibrium, conditions are increasingly recognized to be fundamental controls on fluvial behaviour and stratigraphic architecture (Plink-Björklund, 2015; Reesink et al., 2015; Fielding et al., 2018; Ghinassi et al., 2018; Ganti et al., 2020; Herbert et al., 2020; Leary & Ganti, 2020; Wysocki & Hajek, 2021). At the bedform scale, recent theoretical and experimental observations indicate that fluvial cross strata may preferentially record bedform dynamics in disequilibrium conditions (Reesink et al., 2015; Ganti et al., 2020; Leary & Ganti, 2020), i.e., when flow and bedform evolution are out of phase (c.f. Myrow et al., 2018). Bedform disequilibrium conditions are characterized by localized increase in sedimentation rates relative to the bedform migration rates, which enhances the preservation of bedforms (Reesink et al., 2015; Ganti et al., 2020; Leary & Ganti, 2020). Cross-sets preserved in disequilibrium conditions have diagnostic geometries that deviate from cross-set preservation in steady-state conditions: a) restricted range of cross-set height distributions such that $CV<0.88$ and b) elevated bedform preservation ratios (>0.3) such that a larger fraction of the formative topography is preserved in stratigraphy (Jerolmack & Mohrig, 2005; Leary & Ganti, 2020; Wu et al., 2020).

Two distinct disequilibrium conditions lead to the enhanced preservation of bedforms. First, Leary and Ganti (2020) used experimental data to show characteristic patterns of bedform preservation are found under different conditions of formative flow variability (i.e., the near-instantaneous short-term discharge variability associated with the magnitudes and timescales of individual floods). They demonstrated that preserved cross-sets only have geometries that are consistent with steady-state conditions when the formative flood duration (T_f) is greater than the bedform turnover timescale (T_t) — defined as the time it takes to displace the volume of sediment in a bedform (Myrow et al., 2018). When the formative flood duration is shorter than the bedform turnover timescale, the larger peak flood-equilibrated bedforms get abandoned and are minimally reworked during the flood recession and subsequent low flow conditions, which results in a high bedform preservation ratio and low *CV* for preserved cross-sets (Leary & Ganti, 2020). We term this the *flood hypothesis* for enhanced bedform preservation. Moreover, Leary and Ganti (2020) showed that it is possible to estimate formative flow durations from preserved cross-sets — this may enable quantitative reconstructions of flood variability from the rock record which deviate from traditional qualitative methods that solely rely on facies and architectural models (e.g., Plink-Björklund, 2015). Alternatively, the self-organization of fluvial systems into a morphodynamic hierarchy (e.g., dunes, bars, channels, channel belts) can also cause enhanced preservation of topography with each hierarchical element (Ganti et al., 2020). In this scenario, high bedform preservation ratio and low *CV* can occur due to localized increase in the angle of climb of bedforms associated with, for example, concurrently migrating bedforms and barforms (Jerolmack & Mohrig, 2005; Ganti et al., 2013; Reesink et al., 2015; Ganti et al., 2020). We term this the *hierarchy hypothesis* for enhanced bedform preservation. In both of these scenarios, cross strata are expected to encode more detailed information about morphodynamic conditions in ancient fluvial systems, which are not accounted for in models that assume bedform preservation occurred in steady-state conditions.

Despite advances in understanding bedform dynamics, the prevalence of bedform disequilibrium dynamics in preserved fluvial strata is currently unclear, partly because we lack detailed field measurements of cross-set geometries and their statistical nature. While a handful of field studies have documented low *CV* (0.3–0.7) in fluvial cross strata (Jerolmack & Mohrig, 2005; Colombera et al., 2017; Cardenas et al., 2020; Wang et al., 2020), consistent with bedform disequilibrium dynamics, these data are often limited to a few outcrop observations for individual geologic formations. Here, we systematically characterize the geometries and statistical nature of fluvial cross strata for three Late Cretaceous geologic formations, central Utah, USA (Figs 1,2), to assess the degree to which they reflect bedform disequilibrium dynamics. Across all three formations, we show that fluvial cross strata are dominated by the preservation of bedform disequilibrium dynamics, which contradicts use of steady-state assumptions in palaeohydraulic reconstructions. Using these field observations, we reconstruct bedform kinematics (i.e., turnover timescales) and quantify the formative conditions that are consistent with field data under both the flood and hierarchy hypotheses (i.e., flood durations, migration rates). Finally, we evaluate whether it is possible to deconvolve the relative roles of flood variability and morphodynamic hierarchy on enhanced bedform preservation, which may provide a potentially powerful pathway to reconstruct flood variability in ancient fluvial systems, and to evaluate the nature of interactions between bedforms, bars, channel migration and channel avulsion in palaeo-channel networks.

2. Study area

In the Late Cretaceous North American continent, rivers draining the Sevier orogenic fold-and-thrust belt transported huge volumes of clastic sediments eastwards towards the Western Interior Seaway (WIS) (e.g., Kauffman & Caldwell, 1993) (Fig. 1). We focus on well-studied fluvial strata of the Late Cretaceous Blackhawk Formation, Castlegate Sandstone and Ferron Sandstone in central Utah, USA (Figs 1,2) (c.f. Lyster et al., 2021). These strata have been interpreted to preserve distinct fluvial styles; the Ferron Sandstone represents a major meandering trunk channel (Cotter, 1971; Chidsey et al., 2004), while, at the Blackhawk–Castlegate transition, single- and multi-thread channels of the Blackhawk Formation (Adams & Bhattacharya, 2005; Hampson et al., 2013; Flood & Hampson, 2014) are capped by fully braided channels of the Castlegate Sandstone (Miall, 1993, 1994) (Fig. 1,2). Moreover, these systems are potentially linked with a monsoonal climate (Fricke et al., 2010; Sewall & Fricke, 2013).

2.1 Blackhawk Formation and Castlegate Sandstone, Mesaverde Group

The Campanian Blackhawk Formation and Castlegate Sandstone (Figs 1,2) represent a series of parallel transverse fluvial systems draining the Sevier orogenic front to the WIS (Pettit et al., 2019), with an additional longitudinal component of drainage from the south-southwest (e.g., Szwarc et al., 2015; Pettit et al., 2019) (Fig. 1b). The lower–middle Campanian Blackhawk Formation is a ledge-forming deposit characterized by large fluvial channelized sandstone bodies and abundant floodplain sediments (e.g., Adams & Bhattacharya, 2005; Hampson et al., 2013; Flood & Hampson, 2014) (Fig. 2a–c). These sandstone bodies represent both single- and multi-thread systems, as observed from bar architectures (Adams & Bhattacharya, 2005; Hampson et al., 2013). Meanwhile the middle–upper Campanian Castlegate Sandstone is a cliff-forming deposit situated above the Blackhawk Formation (Fig. 2a) and is characterized by amalgamated braided fluvial channel-belt deposits which, in the middle, are less amalgamated with interbedded mudstones (e.g., Miall, 1993; Miall, 1994). We collected data for the Blackhawk Formation and Castlegate Sandstone from five canyons along the eastern Wasatch Plateau front (Fig. 1a; c.f. Lyster et al. (2021)). Cross-sets in deposits of the Blackhawk Formation are generally associated with both channel thalweg and barform deposits, whereas cross-sets in deposits of the Castlegate Sandstone are predominantly associated with barform deposits (Miall, 1993, 1994; Adams & Bhattacharya, 2005; Hampson et al., 2013; Flood & Hampson, 2014).

2.2 Ferron Sandstone, Mancos Shale

The Turonian Ferron Sandstone comprises three deltaic clastic wedges (Cotter, 1971; Chidsey et al., 2004) (Fig. 1b). These deltas were fed by rivers draining the Sevier orogenic front to the WIS, and may have also featured an additional/intermittent longitudinal component of drainage from the south-southwest, as observed for the Blackhawk Formation–Castlegate Sandstone succession (e.g., Szwarc et al., 2015; Pettit et al., 2019). We focus on the Last Chance deltaic complex, using data from three canyons in southwestern Castle Valley (Fig. 1).

These canyons preserve the most palaeo-landward terrestrial fluvial facies of the Last Chance delta and are characterized by major channelized sandstone bodies and abundant floodplain sediments and palaeosols (Cotter, 1971; Chidsey et al., 2004) (Fig. 2d–f). These strata preserve the major meandering trunk channel that fed the Last Chance delta, which is evidenced by abundant laterally accreted point bar deposits (Cotter, 1971; Chidsey et al., 2004) (Fig. 2f). Cross-sets in these deposits are generally associated with both channel thalweg and point bar deposits (Cotter, 1971; Chidsey et al., 2004).

3. Methods

At field localities, trough and planar cross-sets occurred predominantly in sand-grade sediments and occasionally in coarser granule-grade sediments (Fig. 3). To measure the distribution of heights within individual cross-sets we delineated cross-set boundaries (i.e., the lower, asymptotic bounding surface and the upper, erosional bounding surface) and measured cross-set heights with a vertical precision of ±5 mm at regular intervals along the entire width of the cross-set dip-section (n=5–15 measurements) (Fig. 3e,f), in line with methods outlined in Paola and Borgman (1991), Ganti et al. (2019) and Lyster et al. (2021). We then estimated the median grain-size (D_{50}) using size terms of the Wentworth (1922) classification (Fig. 3a,b). When converted to numerical values, we assigned the middle value for each size term or, where grain-size straddled two size terms, we used the boundary value, e.g., D_{50} of medium-grade sand = 0.375 mm and medium–coarse-grade sand = 0.5 mm (Wentworth, 1922). We repeated this for multiple cross-sets within co-sets. Having measured height distributions within individual cross-sets, we then measured a population of maximum cross-set heights (i.e., the maximum distance between lower and upper bounding surfaces) of cross-sets at each locality (n=~25–75). These cross-sets were all related, spanning multiple co-sets that were confined, where possible, to a single channelized sandstone body.

For each individual cross-set, we calculated the mean cross-set height, h_{xs}, the maximum height, and the *CV* of the internal height distribution ($CV(h_{xs})$) — a key parameter to test whether the bedforms are preserved in steady-state or disequilibrium conditions. For each population of maximum cross-set heights, we similarly calculated the mean maximum cross-set height, h_p, and the *CV* of the entire population ($CV(h_p)$), and we additionally analysed the shape of each distribution.

To evaluate the flood and hierarchy hypotheses, we propagated mean heights of individually measured cross-sets (and their respective grain-sizes) through a quantitative framework to reconstruct bedform turnover timescales. We reconstructed turnover timescales, T_t, i.e., the time taken to displace the volume of sediment of the bedform (per unit width), following Martin and Jerolmack (2013) and Myrow et al. (2018), as:

$$T_t = \frac{\lambda h_d \beta}{q_b}, \qquad \text{[Eq. 1]}$$

where λ is bedform wavelength, h_d is bedform (i.e., dune) height, β ~0.55 is the bedform shape factor and q_b is the unit bedload flux (see Supplementary Methods). As the exact error margins of palaeohydraulic inversion methods are unknown, we used a Monte Carlo uncertainty propagation method to estimate uncertainty, which yielded 10^6 values of T_t per cross-set (Supplementary Methods). From these estimates we extracted median T_t, the 25–75 percentile range of T_t (or the interquartile range of T_t), and the 10–90 percentile range of T_t. We suggest that the 10–90 percentile range of T_t offers plausible minimum and maximum values for median T_t, with the 25–75 percentile range of T_t highlighting where true values of median T_t most likely occur between these bounds. We then performed a two-sample Kolmogorov–Smirnov (K–S) test on the distribution of median T_t reconstructed for each cross-set to determine the statistical similarity of T_t across the three geologic formations.

The reconstruction of T_t requires a priori knowledge of the bedform preservation ratio (h_{xs}/h_d), which itself is a function of whether bedforms were preserved in steady-state or disequilibrium conditions. To evaluate a maximum T_t value, we used h_{xs}/h_d = 0.3, which reflects steady-state preservation under low bedform climb angle. We then assessed the sensitivity of T_t to h_{xs}/h_d by repeating the methodology outlined above for h_{xs}/h_d values from 0 to 1. In the absence of preserved formsets that reflect h_{xs}/h_d >= 1.0 (Reesink et al., 2015), enhanced bedform preservation is characterized by 0.3 < h_{xs}/h_d ≤0.7 (Supplementary Information; Jerolmack and Mohrig (2005); Reesink et al. (2015); Ganti et al. (2020); Leary and Ganti (2020). For the sensitivity analyses, we used the mean h_{xs} and median D_{50} of each measured cross-sets and calculated the overall mean h_{xs} and mean D_{50} for the Blackhawk Formation, Castlegate Sandstone and Ferron Sandstone, respectively.

4. Results

4.1 Cross-set geometries

We present results aggregated at the formation scale, with no spatial or temporal reference frame, as ancillary field observations suggest there is little variation between field sites (see Supplementary Information and Lyster et al. (2021)). We measured >400 individual cross-sets of the Blackhawk Formation (n = 81), Castlegate Sandstone (n = 146) and Ferron Sandstone (n = 190) (Fig. 4), with ~5–15 height measurements per cross-set, totalling >3800 measurements. For each cross-set we recorded grain-size, which is reported in the Supplementary Information. Mean cross-set heights are similar for the Blackhawk Formation and Castlegate Sandstone (p = 0.067; two-sample t-test), with median values of ~0.13–0.14 m and 10–90 percentile ranges of 0.1–0.2 m. Maximum heights for each cross-set have medians of 0.17–0.18 m and 10–90 percentile ranges of 0.13–0.27 m (Fig. 4a,b). For the Ferron Sandstone, cross-sets are larger with broader quartile ranges. Mean cross-set heights have a median of 0.15 m and a 10–90 percentile range of 0.08–0.25 m, and maximum cross-set heights have a median of 0.22 m and a 10–90 percentile range of 0.12–0.45 m (Fig. 4c).

We also measured >3000 maximum cross-set heights across the Blackhawk Formation (801 measurements across 26 populations), Castlegate Sandstone (1015 measurements across 27 populations) and Ferron Sandstone (1257 measurements across 21 populations), with between 25–75 measurements per population (Fig. 5). Of maximum cross-set heights, median values of ~0.2 m (Fig. 5) are consistent with maximum cross-set heights from individually measured cross-set height distributions (Fig. 4). For the Blackhawk Formation and Castlegate Sandstone, 90% of maximum cross-set heights are between ~0.15–0.3 m, and 10% of maximum cross-set heights are relatively larger (≤0.5–0.6 m) (Fig. 5a,c). Meanwhile, for the Ferron Sandstone, 90% of maximum cross-set heights are between ~0.15–0.35 m and 10% of maximum cross-set heights are relatively larger (≤ 0.7 m) (Fig. 5e). These distributions of maximum cross-set heights across all cross-sets are generally mirrored in individual cross-set populations (Fig. 5b,d,f), with median values of ~0.2 m, suggesting they are not from a limited subset of locations. Most populations of maximum cross-set heights demonstrate positively-skewed, long-tailed distributions wherein relatively few large cross-sets exist among abundant smaller cross-sets (Fig 5b,d,f). The kurtosis of distributions varies for each formation, such that distributions in the Castlegate Sandstone and Ferron Sandstone are more long-tailed than in the Blackhawk Formation (Fig 5b,d,f).

Our data show that CV values of cross-set heights are significantly lower than the expected steady-state values of 0.88 (Fig. 6). We found low CV of heights within individual cross-sets ($CV(h_{xs})$), as well as low CV of heights for a population of measured cross-sets within related co-sets ($CV(h_p)$) (Fig. 6). In the Blackhawk Formation and Castlegate Sandstone, median $CV(h_{xs})$ is 0.3 with a 25–75 percentile range of ~0.25–0.38, and maximum $CV(h_{xs})$ extends to 0.45–0.55 (Fig. 6a,b). The Ferron Sandstone $CV(h_{xs})$ values are also low (relative to steady-state) but are higher than in the Blackhawk–Castlegate succession. For the Ferron Sandstone, median $CV(h_{xs})$ is 0.4 with a broader 25–75 percentile range of ~0.3–0.5, and maximum $CV(h_{xs})$ extends to 0.6–0.75 (Fig. 6c). We found that none of the measured $CV(h_{xs})$ values were consistent with the proposed empirical range of 0.88±0.30 for steady-state preservation (Bridge, 1997) in the Blackhawk–Castlegate succession; however, 6% of the measurements were within this range for the Ferron Sandstone. For $CV(h_p)$, recovered values are even lower. In the Blackhawk Formation and Castlegate Sandstone median $CV(h_p)$ is 0.2, with 25–75 percentile ranges of ~0.15–0.25 (Fig. 6a,b), and in the Ferron Sandstone median $CV(h_p)$ is 0.3, with a 25–75 percentile range of ~0.25–0.35 (Fig. 6c).

4.2 Maximum bedform turnover timescales

We first present results for reconstructed T_t values for each formation using a bedform preservation ratio of 0.3, and then explore the sensitivity of T_t to $h_{xs}/h_d > 0.3$ which is expected for the preservation of bedforms under high angles of local bedform climb. The geometries and grain-sizes of measured cross-sets imply that T_t values typically span 1–10 days, with a median value of 2–4 days (Fig. 7). The overall distributions of T_t vary between the geologic formations (Fig. 7). For the Castlegate Sandstone median T_t is 2.5–3 days, with a 10–90 percentile range of 1–7 days (Fig. 7a). For the Blackhawk Formation, values are marginally higher with a median T_t of 3–3.5 days, and a 10–90 percentile range of 1.5–8 days (Fig. 7b).

Statistically, however, T_t values for both the Blackhawk Formation and Castlegate Sandstone are similar as a two-sample K–S test does not reject the null hypothesis (at the 95% confidence interval) that T_t values are drawn from the same underlying distribution. While the Ferron Sandstone has a similar median T_t of 3–3.5 days, it has a much broader 10–90 percentile range spanning <1–15 days (Fig. 7c). When Ferron Sandstone T_t values are contrasted with Blackhawk Formation and Castlegate Sandstone T_t values, respectively, two-sample K–S tests reject the null hypothesis in both instances, indicating that Ferron T_t values are statistically different and sampled from a different underlying distribution.

We recovered 10^6 values of T_t for each cross-set (see Methods and Supplementary Methods) and the results described above present the cumulative distribution function (CDF) of median T_t values for each cross-set (Fig. 7). We also computed the CDFs for the 10^{th}, 25^{th}, 75^{th} and 90^{th} percentiles of T_t values of each cross-set to highlight the plausible range of values that are consistent with field observations. Inclusion of these CDFs demonstrates that, despite uncertainty in T_t of up to one order of magnitude, the vast majority of all possible T_t values are between 1 and 10 days (Fig. 7). These T_t values suggest that typical flood durations >10 days would have fully equilibrated bedforms, similar to modern observations in relatively shallow rivers (Leary & Ganti, 2020). Further, the estimated maximum T_t of 2–4 days, with an overall span of 1–10 days (Fig. 7) for bedforms in the Blackhawk-Castlegate succession and the Ferron sandstone are consistent with modern natural rivers (e.g., Hajek & Straub, 2017; Leary & Ganti, 2020).

4.3 Sensitivity of bedform turnover timescales to bedform preservation ratio

To assess the sensitivity of T_t to h_{xs}/h_d, we systematically varied h_{xs}/h_d for each formation from 0 to 1 (Fig. 8), where the former indicates no preservation and the latter implies the abundance of formset preservation. An increase in h_{xs}/h_d corresponds analytically with a decrease in T_t. For example, increasing h_{xs}/h_d by a factor of 2, from 0.3 to 0.6, reduces T_t by a factor of 5–6 (Fig. 8). Compared to results for h_{xs}/h_d=~0.3, the median T_t values for the Castlegate Sandstone and the Blackhawk Formation are a factor of 5 smaller, with median T_t of 0.7 days (~17 hours) and 1 day, respectively (Figs. 8a, b). For the Ferron Sandstone, h_{xs}/h_d=0.6 reduces the median T_t by a factor of 6 to ~1 day, when compared to h_{xs}/h_d=~0.3 (Fig. 8c). In all cases, extreme dune preservation with h_{xs}/h_d=1 yielded T_t <0.1 days, and extremely low values of h_{xs}/h_d << 0.3 yielded unrealistic T_t values as high as 10^5 days (Fig. 8). Experimental bedform preservation under steady and unsteady flows indicates that the h_{xs}/h_d may likely span 0.3 and 0.7 (grey bars, Fig. 8; Supplementary Information) in the absence of evidence for formset preservation (Leary & Ganti, 2020).

5. Discussion

From >400 individually measured cross-sets (n=5–15 measurements per cross-set) across the three geologic formations, our results indicated that estimated $CV(h_{xs})$ was unanimously lower than 0.88 and ranged from ~0.25–0.5 (Fig. 6). Across these formations, only 3% of the estimated $CV(h_{xs})$ were consistent with the empirical range of 0.88±0.30 expected for bedform preservation under steady-state conditions (Bridge, 1997). Low $CV(h_{xs})$ is inconsistent with steady-state preservation of bedforms and does not support generation of cross-sets by random variability in scour depths through time (Paola & Borgman, 1991; Leclair & Bridge, 2001; Leclair, 2002; Jerolmack & Mohrig, 2005). Instead, our observations provide evidence for enhanced bedform preservation driven by localized increase in sedimentation rates relative to the bedform migration rates (Jerolmack & Mohrig, 2005; Ganti et al., 2020; Leary & Ganti, 2020), suggesting that fluvial deposits of the Blackhawk Formation, Castlegate Sandstone, and Ferron Sandstone are dominated by bedform disequilibrium dynamics. Below we discuss the implications of these observations under the flood and hierarchy hypotheses, and delineate potential approaches to disentangle their relative roles in ancient fluvial systems.

5.1 Implications of the flood hypothesis for bedform preservation

Using physical experiments, Leary and Ganti (2020) showed that, where bedform disequilibrium dynamics are only controlled by formative flow variability, low $CV(h_{xs})$ indicates a scenario in which the formative flood duration (T_f) is significantly less than the bedform turnover timescale (T_t). Bedform disequilibrium dynamics associated with formative flow variability typically manifest in rivers with flashy flood hydrographs, in which river discharge is characterized by floods with a short flood recession period relative to T_t (Leary & Ganti, 2020) — the rapid decline in water discharge following peak flood minimizes bedform reworking and enhances bedform preservation (Leary & Ganti, 2020). Under the flood hypothesis, the documented low $CV(h_{xs})$ is consistent with T_f values that are a factor of 10 smaller than T_t (assuming the ratio of T_f to T_t is ~0.1; c.f. Leary and Ganti (2020)). As the maximum T_t values fall between 1–10 days for our field data, the estimated $CV(h_{xs})$ indicates typical T_f values spanning 0.1–1 day (2.4–24 hours) for h_{xs}/h_d=~0.3. The range of plausible T_f values consistent with experimentally observed bedform preservation ratios and field-estimated $CV(h_{xs})$ are on the order of 0.1 days for all the geologic formations considered here (Fig. 8).

Under the flood hypothesis, our field data unanimously indicate that the typical formative flood durations did not exceed a few hours to a day for these Late Cretaceous fluvial systems. Our estimated flood durations are plausible and consistent with recent (decadal-scale) observations of modern rivers in sub-tropical and/or mid-latitude regions (e.g., Serinaldi et al., 2018). Moreover, compilations of global flood data indicate that, for flood durations of order hours to days, the main causes are: heavy rain, brief torrential rain, tropical storms, and extra-tropical storms (Serinaldi et al., 2018). These flood durations, and associated causes, are typical of perennial discharge regimes. While the Blackhawk Formation, Castlegate Sandstone and Ferron Sandstone have not been explicitly studied in terms of variable discharge facies models, existing facies analyses of these formations have typically described sedimentary and architectural structures associated with perennial rivers (see review by

Plink-Björklund, 2015). These include abundant Froude subcritical structures (i.e., cross-sets from which we collected data; Fig. 3) and well-developed macroforms (i.e., barforms and accretion sets) (Cotter, 1971; Miall, 1994; Chidsey et al., 2004; Adams & Bhattacharya, 2005; Hampson et al., 2013; Flood & Hampson, 2014; Chamberlin & Hajek, 2019).

Independent modelling and proxy studies of palaeoclimate in Late Cretaceous central Utah suggest the region was subject to a sub-tropical/monsoonal climate with monsoonal precipitation and frequent seasonal flooding in low-lying alluvial plains (e.g., Fricke et al., 2010; Sewall & Fricke, 2013). However, floods caused by monsoonal rains typically have long durations spanning ~5–25 days (Serinaldi et al., 2018). Additionally, an abundance of features associated with monsoonal systems, e.g., in-channel mud layers, abundant soft-sediment deformation, soft-sediment clast conglomerates (see review by Plink-Björklund, 2015), have not been reported in literature for these formations or observed at our field localities. Given that our reconstructed flood durations and existing facies models indicate perennial discharge regimes, the flood hypothesis indicates that these fluvial deposits could record bedform adjustment to flooding associated with storm events as opposed to sustained monsoonal flooding.

5.2 Implications of the hierarchy hypothesis for bedform preservation

Under the alternative hierarchy hypothesis, enhanced bedform preservation is facilitated by self-organization of fluvial systems into a series of hierarchical elements (Ganti et al., 2020), where the nature of preservation of topography within a given hierarchical level is solely controlled by the next level in the morphodynamic hierarchy. The presence of unit bars and barforms — the higher-order hierarchical elements of dunes — will locally enhance preservation of river dunes because the bars both provide accommodation for bedforms and increase bedform climb angles (Reesink et al., 2015; Ganti et al., 2020). Cardenas et al. (2020) observed low $CV(h_{xs})$ for bedforms preserved on the stoss and lee slopes of barforms, when compared to bedforms preserved in thalweg deposits of the Cretaceous Cedar Mountain Formation, Utah, which is consistent with the hierarchy hypothesis for bedform preservation. Numerical models indicate that observed low $CV(h_{xs})$ values are associated with rapid sedimentation rates relative to bedform migration rates such that the bedform climb angle is of the order of 10^{-2} to 10^{-1} (Jerolmack & Mohrig, 2005). Given that the local angle of climb for bedforms is influenced by the relative rates of dune migration to bar migration (Ganti et al., 2020), these results suggest low $CV(h_{xs})$ values measured in the field are consistent with timescales of bar migration on the order of days to months.

The nature of stratigraphic architecture, particularly of barform deposits, is well-documented for the Blackhawk Formation, Castlegate Sandstone and Ferron Sandstone (Cotter, 1971; Miall, 1993, 1994; Chidsey et al., 2004; Adams & Bhattacharya, 2005; Hampson et al., 2013; Flood & Hampson, 2014; Chamberlin & Hajek, 2019; Lyster et al., 2021). The Castlegate Sandstone comprises amalgamated fluvial channel-belt deposits which, architecturally, are dominated by barforms (e.g., mid-channel bars) (Miall, 1993, 1994; Chamberlin & Hajek, 2019). Therefore, cross-sets that we measured in the Castlegate Sandstone likely preserve bedforms that were influenced by barform migration, and it is possible that low $CV(h_{xs})$ values observed in these cross-sets reflect bedform disequilibrium dynamics associated with the hierarchy hypothesis, especially given that unit bar migration typical of braided rivers can be comparable to dune migration rates (Strick et al., 2019). Conversely, fluvial strata of the Blackhawk Formation and Ferron Sandstone comprise major channelized sandstone bodies (Cotter, 1971; Chidsey et al., 2004; Adams & Bhattacharya, 2005; Hampson et al., 2013; Flood & Hampson, 2014) which, while abundant in barforms (e.g., laterally accreted point bar deposits; Fig. 2f), also likely preserve a much larger proportion of channel deposits that are devoid of barform architecture, and which may reflect thalweg deposits. Therefore, we hypothesize that low $CV(h_{xs})$ values observed in preserved cross-sets of the Blackhawk Formation and Ferron Sandstone, particularly the latter thalweg deposits, may be less likely to reflect bedform preservation in the presence of rapid bar migration.

5.3 Detangling flood versus hierarchy controls on bedform preservation

While both the flood hypothesis and the hierarchy hypothesis explain the observed dominance of enhanced bedform preservation, disentangling their relative roles in controlling bedform preservation is currently non-trivial. We hypothesize that spatially contextualizing the observed deposits may be critical for evaluating the controls on bedform preservation. For example, it is likely that bedforms preserved in channel-thalweg deposits of single-thread rivers are not influenced by the presence of barforms and, therefore, may reflect the formative flood variability. This scenario may be similar to physical experiments that are devoid of multiple morphodynamic hierarchical levels that typify natural rivers. Similarly, field observations indicate that bedforms preserved in the presence of bars are likely to be better preserved than expected under steady-state conditions (Reesink et al., 2015; Cardenas et al., 2020). In this scenario, $CV(h_{xs})$ may yield insight into the relative rates at which bedforms and barforms migrated in ancient fluvial systems. Together, single-thread river deposits may display a larger range of $CV(h_{xs})$ that reflects both formative flood variability and the relative kinematic rates of evolution of successive hierarchical levels in the morphodynamic hierarchy. In contrast, braided rivers are characterized by relatively rapid migration of unit bars and free bars in the presence of river dunes (e.g., Strick et al., 2019) and detangling the role of morphodynamic hierarchy and flood variability may be more difficult. Our results are consistent with this expectation as we observe a larger range of $CV(h_{xs})$ for single-thread river deposits of the Ferron Sandstone compared to the braided river deposits of the Castlegate Sandstone (Fig. 6).

In terms of cross-set geometries, a promising avenue to decipher the dominant control on bedform disequilibrium dynamics is to compare population statistics of related cross-sets, measured in the field, with those from experimental observations. For instance, Leary and Ganti (2020) showed that, in flashy flood hydrographs, the rapid decline of water discharge associated with short waning-flow durations enhances preservation of relatively larger, peak-flood equilibrated, bedforms (Leary & Ganti, 2020). In this scenario, we expect maximum cross-set heights to have a positively-skewed long-tailed distribution with large cross-sets interspersed with relatively smaller cross-sets (Leary & Ganti, 2020). Whereas bedform preservation in steady-state conditions, or under a broad flood hydrograph, will likely result in maximum cross-set heights that have a short-tailed distribution, with a much higher frequency of smaller cross-sets, as longer waning-flow durations enable reworking of larger bedforms such that the preservation potential of peak-flood equilibrated bedforms is low (Leclair, 2011; Leary & Ganti, 2020). Our distributions of maximum cross-set heights for individual populations (Fig. 5b,d,f) are consistent with bedform preservation under the flood hypothesis; most populations have long-tailed, positively skewed distributions (Figs 5b,f). Based on these considerations, we judge it plausible that fluvial stratigraphy in the Blackhawk Formation and Ferron Sandstone may record bedform disequilibrium dynamics driven by formative flow variability, associated with the magnitudes and timescales of individual discharge events on the timescale of hours to days. Future experimental and modelling work should investigate whether and how bedform preservation ratios and the statistical nature of preserved cross-sets differs between systems in which bedform disequilibrium dynamics are driven by flashy flood hydrographs versus coevolution of bedforms and bars, respectively. We advocate that this is the next step in determining the extent to which discharge variability can be quantitatively reconstructed from stratigraphic observables.

Ultimately, despite sampling a variety of fluvial planform styles across large geographic regions, our results indicate that measured cross-set geometries do not comply with the geometries expected for bedform preservation under steady-state conditions, which routinely underpin palaeohydraulic investigations of ancient fluvial systems. This indicates that the bedform preservation ratios often assumed in the field (~0.3) may overestimate true palaeoflow depths (c.f. Leclair & Bridge, 2001) and consequently underestimate palaeoslopes. We argue that systematic measurements of cross-set geometries and, where possible, bedform preservation ratios should be a routine tool to facilitate and contextualize palaeohydraulic reconstructions, and to test for the presence of bedform disequilibrium dynamics.

6. Conclusions

We made systematic measurements of cross-set geometries and grain-sizes in fluvial strata of three Late Cretaceous geologic formations in central Utah, USA: the Blackhawk Formation, Castlegate Sandstone, and Ferron Sandstone. Across all three formations, we documented unanimously low $CV(h_{xs})$ in preserved cross-set heights of 0.25–0.5. These field observations are inconsistent with the steady-state bedform preservation model that assumes cross-sets are generated by random variability in scour depth with time (Paola & Borgman, 1991; Leclair & Bridge, 2001). Instead, our observations add to the growing recognition that bedform preservation is dominated by disequilibrium dynamics (Reesink et al., 2015; Ganti et al., 2020;

Leary & Ganti, 2020), resulting in higher bedform preservation ratios and the deposition of cross-sets which preserve a relatively narrow distribution of heights ($CV(h_{xs})$<<0.88).

We considered two independent hypotheses that lead to enhanced bedform preservation in disequilibrium conditions. Under the flood hypothesis, our data indicate that the formative flood durations that typify these deposits likely ranged from hours to days, which are reflective of heavy rain and tropical storms in these ancient fluvial landscapes. Under the hierarchy hypothesis, the observed low $CV(h_{xs})$ is consistent with bedform deposits preserved with rapidly evolving barforms whose timescale of migration likely spans days to months. Detangling the flood versus hierarchy controls on bedform preservation may be possible through the spatial contextualization of preserved deposits of single-thread rivers, with flood variability potentially the dominant control on the nature of bedform preservation in channel-thalweg deposits, such as those observed in the Ferron Sandstone and Blackhawk Formation. However, detangling these relative controls may be difficult in the deposits of braided rivers, such as the Castlegate Sandstone, that are characterized by relatively rapid migration of unit bars and braid bars that can lead to the enhanced bedform preservation.

Where low $CV(h_{xs})$ reflects enhanced bedform preservation associated with formative flood variability, the approaches presented in this paper have significant implications for investigating discharge variability in the geologic past, particularly the magnitudes, transport capacities, and durations of individual flood events generated during short-period climatic perturbations. Meanwhile, where low $CV(h_{xs})$ reflects enhanced bedform preservation associated with the presence of a morphodynamic hierarchy, these results have implications for evaluating the nature of interactions between bedforms, bars, channel migration and channel avulsion in palaeo-channel networks. We advocate that quantifying cross-set geometries should become a standard approach in future studies to improve and contextualize palaeohydrological reconstructions from ancient fluvial deposits.

Acknowledgements

This research was primarily funded by a Natural Environment Research Council (NERC) Science and Solutions for a Changing Planet Doctoral Training Partnership (DTP) grant to SJL, with additional funding by The Geological Society of London and The British Sedimentological Research Group to SJL. We thank George Hedley and Bailey Lathrop for support with field data collection, and we thank the Safiya Alpheus for useful discussions.

Author Contributions

SJL and ACW designed the study. SJL and ACW conducted field data collection. SJL processed and analysed field data. SJL, ACW, EAH and VG analysed and interpreted results. SJL wrote the manuscript, and ACW, EAH and VG all contributed significantly to the manuscript.

Competing Interests

The authors declare no competing interests.

Data Availability

Field data available in the Supplementary Information.

References

Adams, M. M., & Bhattacharya, J. P. (2005). No change in fluvial style across a sequence boundary, Cretaceous Blackhawk and Castlegate formations of central Utah, U.S.A. *Journal of Sedimentary Research, 75*(6), 1038-1051. doi:10.2110/jsr.2005.080

Allen, J. R. L. (1982). *Sedimentary Structures; Their Character and Physical Basis. Volume I* (Vol. 30). Amsterdam: Elsevier.

Best, J. (2005). The fluid dynamics of river dunes: A review and some future research directions. *Journal of Geophysical Research: Earth Surface, 110*(F4). doi:10.1029/2004JF000218

Bradley, R. W., & Venditti, J. G. (2017). Reevaluating dune scaling relations. *Earth-Science Reviews, 165*, 356-376. doi:10.1016/j.earscirev.2016.11.004

Bridge, J. S. (1997). Thickness of sets of cross strata and planar strata as a function of formative bed-wave geometry and migration, and aggradation rate. *Geology, 25*(11), 971-974. doi:10.1130/0091-7613(1997)025<0971:TOSOCS>2.3.CO;2

Cardenas, B. T., Mohrig, D., Goudge, T. A., Hughes, C. M., Levy, J. S., Swanson, T., . . . Zhao, F. (2020). The anatomy of exhumed river-channel belts: Bedform to belt-scale river kinematics of the Ruby Ranch Member, Cretaceous Cedar Mountain Formation, Utah, USA. *Sedimentology, 67*(7), 3655-3682. doi:10.1111/sed.12765

Carling, P. A. (1999). Subaqueous gravel dunes. *Journal of Sedimentary Research, 69*(3), 534-545. doi:10.2110/jsr.69.534

Chamberlin, E. P., & Hajek, E. A. (2019). Using bar preservation to constrain reworking in channel-dominated fluvial stratigraphy. *Geology, 47*(6), 531-534. doi:10.1130/G46046.1

Chidsey, T. C., Adams, R. D., & Morris, T. H. (2004). *Regional to Wellbore Analog for Fluvial-Deltaic Reservoir Modeling: The Ferron Sandstone of Utah* (Vol. 50).

Colombera, L., Arévalo, O. J., & Mountney, N. P. (2017). Fluvial-system response to climate change: The Paleocene-Eocene Tremp Group, Pyrenees, Spain. *Global and Planetary Change, 157*, 1-17. doi:10.1016/j.gloplacha.2017.08.011

Cotter, E. (1971). Paleoflow characteristics of a late Cretaceous river in Utah from analysis of sedimentary structures in the Ferron sandstone. *Journal of Sedimentary Research, 41*, 129–138. doi:10.1306/74D72202-2B21-11D7-8648000102C1865D

Edgar, L. A., Gupta, S., Rubin, D. M., Lewis, K. W., Kocurek, G. A., Anderson, R. B., . . . Williams, A. J. (2018). Shaler: in situ analysis of a fluvial sedimentary deposit on Mars. *Sedimentology, 65*(1), 96-122. doi:10.1111/sed.12370

Fielding, C. R., Alexander, J., & Allen, J. P. (2018). The role of discharge variability in the formation and preservation of alluvial sediment bodies. *Sedimentary Geology, 365*, 1-20. doi:10.1016/j.sedgeo.2017.12.022

Flood, Y. S., & Hampson, G. J. (2014). Facies and architectural analysis to interpret avulsion style and variability: Upper Cretaceous Blackhawk Formation, Wasatch Plateau, central Utah, U.S.A. *Journal of Sedimentary Research, 84*(9), 743-762. doi:10.2110/jsr.2014.59

Foreman, B. Z., Heller, P. L., & Clementz, M. T. (2012). Fluvial response to abrupt global warming at the Palaeocene/Eocene boundary. *Nature, 491*, 92-95. doi:10.1038/nature11513

Fricke, H. C., Foreman, B. Z., & Sewall, J. O. (2010). Integrated climate model-oxygen isotope evidence for a North American monsoon during the Late Cretaceous. *Earth and Planetary Science Letters, 289*(1-2), 11-21. doi:10.1016/j.epsl.2009.10.018

Ganti, V., Hajek, E. A., Leary, K., Straub, K. M., & Paola, C. (2020). Morphodynamic hierarchy and the fabric of the sedimentary record. *Geophysical Research Letters, 47*(14), e2020GL087921. doi:10.1029/2020GL087921

Ganti, V., Paola, C., & Foufoula-Georgiou, E. (2013). Kinematic controls on the geometry of the preserved cross sets. *Journal of Geophysical Research: Earth Surface, 118*(3), 1296-1307. doi:10.1002/jgrf.20094

Ganti, V., Whittaker, A., Lamb, M. P., & Fischer, W. W. (2019). Low-gradient, single-threaded rivers prior to greening of the continents. *Proceedings of the National Academy of Sciences, 116*(4), 11652-11657. doi:10.1073/pnas.1901642116

Gardner, M. H., Cross, T. A., & Levorsen, M. (2004). Stacking Patterns, Sediment Volume Partitioning, and Facies Differentiation in Shallow-Marine and Coastal-Plain Strata of the Cretaceous Ferron Sandstone, Utah. In T. C. Chidsey, Jr., R. D. Adams, & T. H. Morris (Eds.), Regional to Wellbore Analog for Fluvial-Deltaic Reservoir Modeling: The Ferron Sandstone of Utah (Vol. 50, pp. 0): American Association of Petroleum Geologists. doi:10.1306/St50983

Garrison, J. R., Jr., & Bergh, T. C. V. v. d. (2004). High-Resolution Depositional Sequence Stratigraphy of the Upper Ferron Sandstone Last Chance Delta: An Application of Coal-Zone Stratigraphy. In T. C. Chidsey, Jr., R. D. Adams, & T. H. Morris (Eds.), Regional to Wellbore Analog for Fluvial-Deltaic Reservoir Modeling: The Ferron Sandstone of Utah (Vol. 50, pp. 0): American Association of Petroleum Geologists. doi:10.1306/St50983

Ghinassi, M., Moody, J., & Martin, D. (2018). Influence of extreme and annual floods on point-bar sedimentation: Inferences from Powder River, Montana, USA. *GSA Bulletin, 131*(1-2), 71-83. doi:10.1130/B31990.1

Hajek, E. A., & Heller, P. L. (2012). Flow-depth scaling in alluvial architecture and nonmarine sequence stratigraphy: Example from the Castlegate Sandstone, central Utah, U.S.A. *Journal of Sedimentary Research, 82*(2), 121-130. doi:10.2110/jsr.2012.8

Hajek, E. A., & Straub, K. M. (2017). Autogenic sedimentation in clastic stratigraphy. *Annual Review of Earth and Planetary Sciences, 45*(1), 681-709. doi:10.1146/annurev-earth-063016-015935

Hampson, G. J., Jewell, T. O., Irfan, N., Gani, M. R., & Bracken, B. (2013). Modest change in fluvial style with varying accommodation in regressive alluvial-to-coastal-plain wedge: Upper Cretaceous Blackhawk Formation, Wasatch Plateau, central Utah, U.S.A. *Journal of Sedimentary Research, 83*(2), 145-169. doi:10.2110/jsr.2013.8

Herbert, C. M., Alexander, J., Amos, K. J., & Fielding, C. R. (2020). Unit bar architecture in a highly-variable fluvial discharge regime: Examples from the Burdekin River, Australia. *Sedimentology, 67*(1), 576-605. doi:10.1111/sed.12655

Holbrook, J., & Wanas, H. (2014). A fulcrum approach to assessing source-to-sink mass balance using channel paleohydrologic paramaters derivable from common fluvial data sets with an example from the Cretaceous of Egypt. *Journal of Sedimentary Research, 84*(5), 349-372. doi:10.2110/jsr.2014.29

Jerolmack, D. J., & Mohrig, D. (2005). Frozen dynamics of migrating bedforms. *Geology, 33*(1), 57-60. doi:10.1130/G20897.1

Kauffman, E. G., & Caldwell, W. (1993). The Western Interior Basin in space and time. In E. G. Kauffman & W. Caldwell (Eds.), *Evolution of the Western Interior Basin: Geological Association of Canada, Special Paper 39* (pp. 1-30).

Leary, K. C. P., & Ganti, V. (2020). Preserved fluvial cross strata record bedform disequilibrium dynamics. *Geophysical Research Letters, 47*(2), e2019GL085910. doi:10.1029/2019GL085910

Leclair, S. F. (2002). Preservation of cross-strata due to the migration of subaqueous dunes: an experimental investigation. *Sedimentology, 49*(6), 1157-1180. doi:10.1046/j.1365-3091.2002.00482.x

Leclair, S. F. (2011). Interpreting Fluvial Hydromorphology from the Rock Record: Large-River Peak Flows Leave No Clear Signature. In S. K. Davidson, S. Leleu, & C. P. North (Eds.), From River to Rock Record: The preservation of fluvial sediments and their subsequent interpretation (Vol. 97, pp. 0): SEPM Society for Sedimentary Geology. doi:10.2110/sepmsp.097.113

Leclair, S. F., & Bridge, J. S. (2001). Quantitative interpretation of sedimentary structures formed by river dunes. *Journal of Sedimentary Research, 71*(5), 713-716. doi:1527-1404/01/071-713/$03.00

Lynds, R., & Hajek, E. (2006). Conceptual model for predicting mudstone dimensions in sandy braided-river reservoirs. *AAPG Bulletin, 90*(8), 1273-1288. doi:10.1306/03080605051

Lyster, S. J., Whittaker, A. C., Hampson, G. J., Hajek, E. A., Allison, P. A., & Lathrop, B. A. (2021). Reconstructing the morphologies and hydrodynamics of ancient rivers from source to sink: Cretaceous Western Interior Basin, Utah, USA. *Sedimentology*. doi:10.1111/sed.12877

Mahon, R. C., & McElroy, B. (2018). Indirect estimation of bedload flux from modern sand-bed rivers and ancient fluvial strata. *Geology, 46*(7), 579-582. doi:10.1130/G40161.1

Martin, R. L., & Jerolmack, D. J. (2013). Origin of hysteresis in bed form response to unsteady flows. *Water Resources Research, 49*(3), 1314-1333. doi:10.1002/wrcr.20093

McLaurin, B. T., & Steel, R. J. (2007). Architecture and origin of an amalgamated fluvial sheet sand, lower Castlegate Formation, Book Cliffs, Utah. *Sedimentary Geology, 197*(3), 291-311. doi:10.1016/j.sedgeo.2006.10.005

Miall, A. D. (1993). The architecture of fluvial-deltaic sequences in the Upper Mesaverde Group (Upper Cretaceous), Book Cliffs, Utah. *Geological Society, London, Special Publications, 75*(1), 305. doi:10.1144/GSL.SP.1993.075.01.19

Miall, A. D. (1994). Reconstructing fluvial macroform architecture from two-dimensional outcrops; examples from the Castlegate Sandstone, Book Cliffs, Utah. *Journal of Sedimentary Research, 64*(2b), 146-158. doi:10.1306/D4267F78-2B26-11D7-8648000102C1865D

Myrow, P. M., Jerolmack, D. J., & Perron, J. T. (2018). Bedform disequilibrium. *Journal of Sedimentary Research, 88*(9), 1096-1113. doi:10.2110/jsr.2018.55

Paola, C., & Borgman, L. (1991). Reconstructing random topography from preserved stratification. *Sedimentology, 38*(4), 553-565. doi:10.1111/j.1365-3091.1991.tb01008.x

Pettit, B. S., Blum, M., Pecha, M., McLean, N., Bartschi, N. C., & Saylor, J. E. (2019). Detrital-zircon U-Pb paleodrainage reconstruction and geochronology of the Campanian Blackhawk–Castlegate succession, Wasatch Plateau and Book Cliffs, Utah, U.S.A. *Journal of Sedimentary Research, 89*(4), 273-292. doi:10.2110/jsr.2019.18

Plink-Björklund, P. (2015). Morphodynamics of rivers strongly affected by monsoon precipitation: Review of depositional style and forcing factors. *Sedimentary Geology, 323*, 110-147. doi:10.1016/j.sedgeo.2015.04.004

Reesink, A. J. H., Van den Berg, J. H., Parsons, D. R., Amsler, M. L., Best, J. L., Hardy, R. J., . . . Szupiany, R. N. (2015). Extremes in dune preservation: Controls on the completeness of fluvial deposits. *Earth-Science Reviews, 150*, 652-665. doi:10.1016/j.earscirev.2015.09.008

Romans, B. W., Castelltort, S., Covault, J. A., Fildani, A., & Walsh, J. P. (2016). Environmental signal propagation in sedimentary systems across timescales. *Earth-Science Reviews, 153*, 7-29. doi:10.1016/j.earscirev.2015.07.012

Serinaldi, F., Loecker, F., Kilsby, C. G., & Bast, H. (2018). Flood propagation and duration in large river basins: a data-driven analysis for reinsurance purposes. *Natural Hazards, 94*(1), 71-92. doi:10.1007/s11069-018-3374-0

Sewall, J. O., & Fricke, H. C. (2013). Andean-scale highlands in the Late Cretaceous Cordillera of the North American western margin. *Earth and Planetary Science Letters, 362*, 88-98. doi:10.1016/j.epsl.2012.12.002

Straub, K. M., Duller, R. A., Foreman, B. Z., & Hajek, E. A. (2020). Buffered, incomplete, and shredded: The challenges of reading an imperfect stratigraphic record. *Journal of Geophysical Research: Earth Surface, 125*(3), e2019JF005079. doi:10.1029/2019JF005079

Strick, R. J. P., Ashworth, P. J., Sambrook Smith, G. H., Nicholas, A. P., Best, J. L., Lane, S. N., . . . Dale, J. (2019). Quantification of bedform dynamics and bedload sediment flux in sandy braided rivers from airborne and satellite imagery. *Earth Surface Processes and Landforms, 44*(4), 953-972. doi:10.1002/esp.4558

Szwarc, T. S., Johnson, C. L., Stright, L. E., & McFarlane, C. M. (2015). Interactions between axial and transverse drainage systems in the Late Cretaceous Cordilleran foreland basin: Evidence from detrital zircons in the Straight Cliffs Formation, southern Utah, USA. *GSA Bulletin, 127*(3-4), 372-392. doi:10.1130/B31039.1

Ten Brinke, W. B. M., Wilbers, A. W. E., & Wesseling, C. (1999). Dune Growth, Decay and Migration Rates during a Large-Magnitude Flood at a Sand and Mixed Sand–Gravel Bed in the Dutch Rhine River System. *Fluvial Sedimentology VI*, 15-32. doi:10.1002/9781444304213.ch2

Trampush, S. M., Huzurbazar, S., & McElroy, B. (2014). Empirical assessment of theory for bankfull characteristics of alluvial channels. *Water Resources Research, 50*(12), 9211-9220. doi:10.1002/2014WR015597

van Rijn, L. C. (1984). Sediment transport III: bedforms and alluvial roughness. *Journal of Hydraulic Engineering, 110*(12), 1733-1754. doi:10.1061/(ASCE)0733-9429(1984)110:12(1733)

Wang, R., Colombera, L., & Mountney, N. P. (2020). Palaeohydrological characteristics and palaeogeographic reconstructions of incised-valley-fill systems: Insights from the Namurian successions of the United Kingdom and Ireland. *Sedimentology, n/a*(n/a). doi:10.1111/sed.12773

Wentworth, C. K. (1922). A scale of grade and class terms for clastic sediments. *The Journal of Geology, 30*(5), 377-392. doi:10.1086/622910

Wu, C., Nittrouer, J. A., Swanson, T., Ma, H., Barefoot, E., Best, J., & Allison, M. (2020). Dune-scale cross-strata across the fluvial-deltaic backwater regime: Preservation potential of an autogenic stratigraphic signature. *Geology, 48*(12), 1144-1148. doi:10.1130/G47601.1

Wysocki, N., & Hajek, E. A. (2021). Mud in sandy riverbed deposits as a proxy for ancient fine-sediment supply. *Geology*. doi:10.1130/G48251.1

Figures

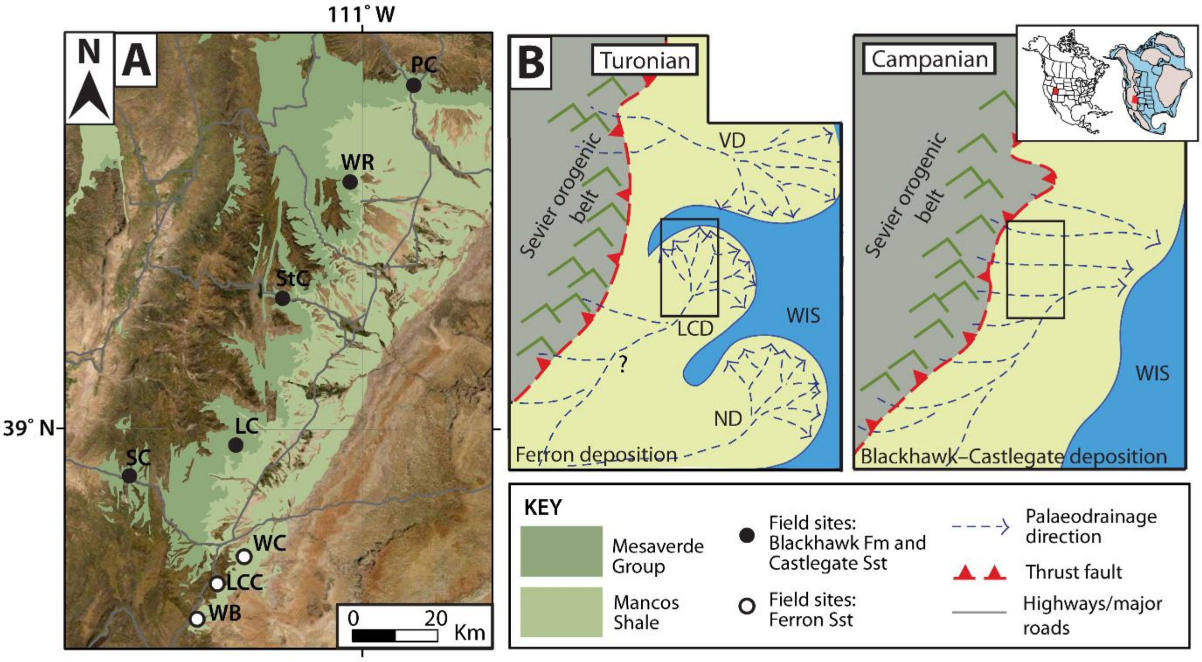

Figure 1: Study area. A) Field areas in central Utah, U.S.A., which include Last Chance Creek (LCC), Link Canyon (LC), Price Canyon (PC), Salina Canyon (SC), Straight Canyon (StC), Wattis Road (WR), Willow Basin (WB) and Willow Creek (WC). LC, PC, SC, StC and WR are field sites from which we obtained data for the Blackhawk Formation and Castlegate Sandstone (Mesaverde Group; black-filled circles). LCC, WB and WC are field sites from which we obtained data for the Ferron Sandstone (Mancos Shale; white-filled circles). B) A conceptual diagram of Utah palaeogeography and palaeodrainage in both the Turonian (left) and Campanian (right). Likely palaeodrainage configurations (and delta progradation) are indicated by dashed blue lines with arrows. The black outlined box in the centre of each palaeogeography indicates the study area (i.e., the approximate position and extent of A). The location of Utah relative to the modern North American continent (left) and the Late Cretaceous North American continent (right) is shown in the inset figure — Utah is highlighted as a red box. LCD = Last Chance delta; ND = Notom delta; VD = Vernal delta; WIS = Western Interior Seaway. Figure adapted from Lyster et al. (2021).

[2 column figure]

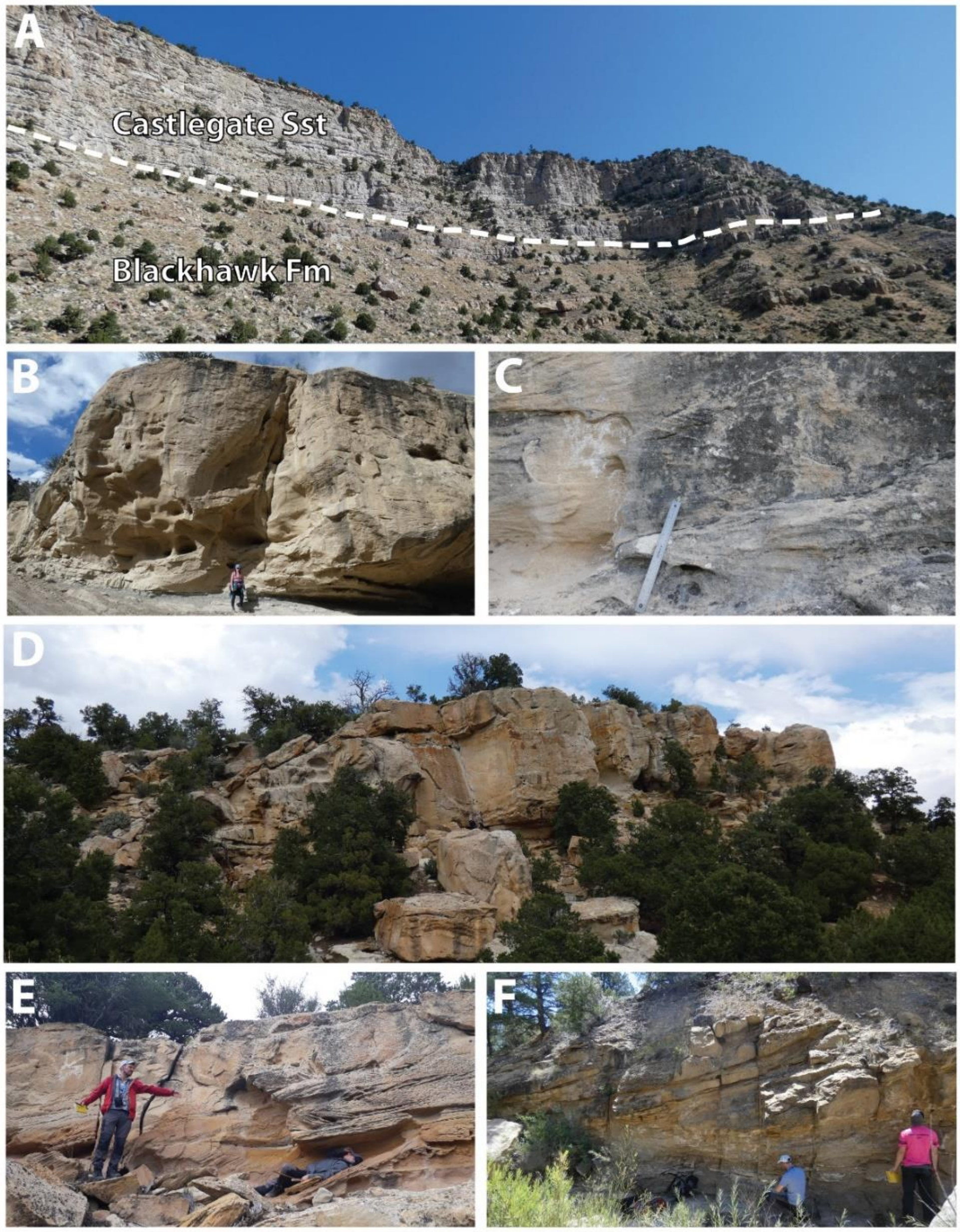

Figure 2: An overview of Upper Cretaceous fluvial strata from which we collected field data in central Utah, USA. A) Example of typical exposure of the Blackhawk Formation and Castlegate Sandstone (at Salina Canyon; SC; Fig. 1) which crops out in canyons along the eastern Wasatch front. Dashed white line indicates the lithostratigraphic boundary between the Blackhawk Formation and Castlegate Sandstone. B) Example of a major channelized fluvial sandstone body of the Blackhawk Formation at Link Canyon (LC; Fig. 1). C) Crude cross-stratification of amalgamated fluvial deposits of the Castlegate Sandstone at Price Canyon (PC; Fig. 1). D) Example of a major channelized sandstone body of the Ferron Sandstone at Last Chance Creek (LCC; Fig. 1). Persons for scale in centre of image. E) Cross-stratified fluvial strata of the Ferron Sandstone at LCC (with some soft-sediment deformation apparent). F) Laterally accreted point bar deposits of the Ferron Sandstone at LCC.

[2 column figure]

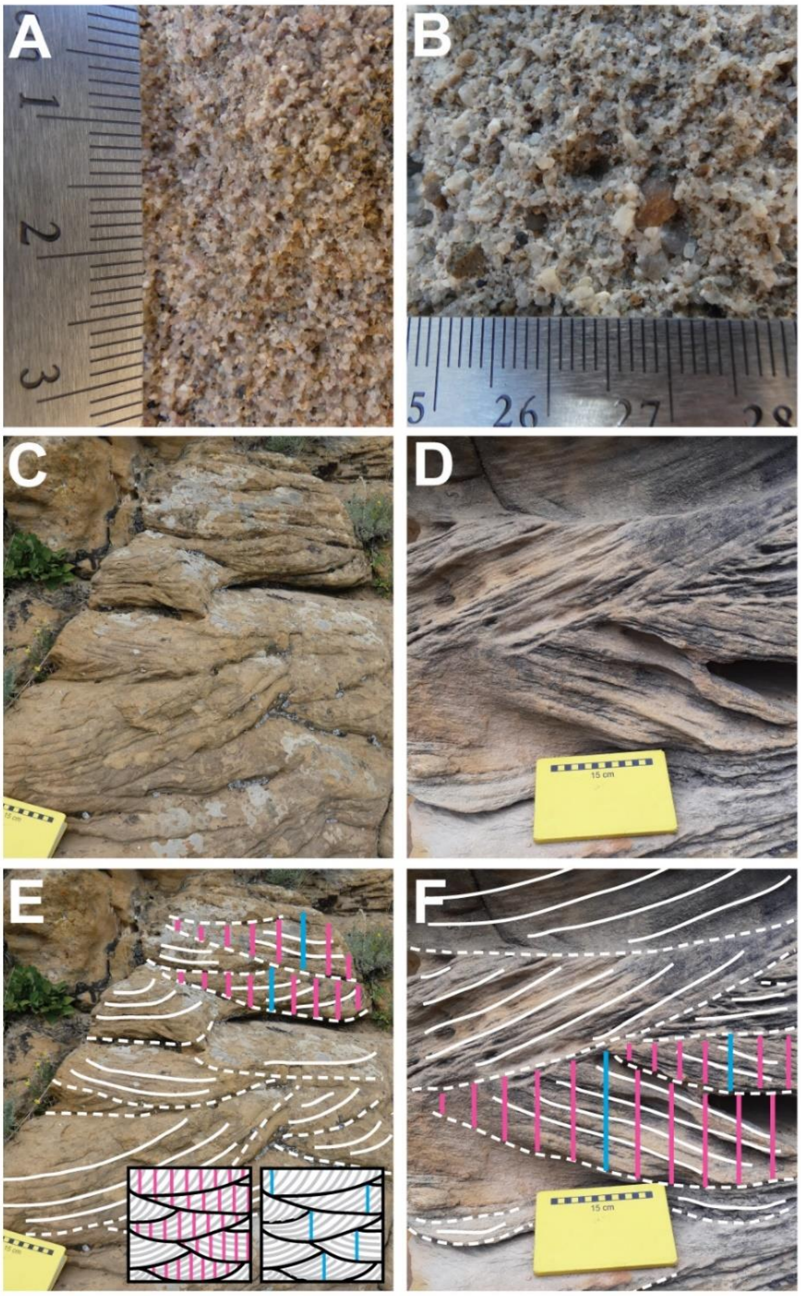

Figure 3: Field methods. A,B) For each measured cross-set, grain-size was assigned using the Wentworth (1922) classification. C,D) Examples of cross-sets from which distributions of cross-set heights were measured. E,F) Interpreted versions of the images in C,D. Dashed white lines indicate bounding surfaces between cross-sets and solid white lines indicate individual foresets within cross-sets. To exemplify how cross-sets were measured, pink vertical lines indicate the regular spacing within individual cross-sets at which heights were measured, and blue vertical lines indicate where maximum cross-set heights would have been measured for a population of cross-sets within co-sets at each locality. Insets in E are schematic representations of these two methods of data collection from cross-sets using pink and blue lines, respectively. Figure adapted from Lyster et al. (2021).

[1 or 1.5 column figure]

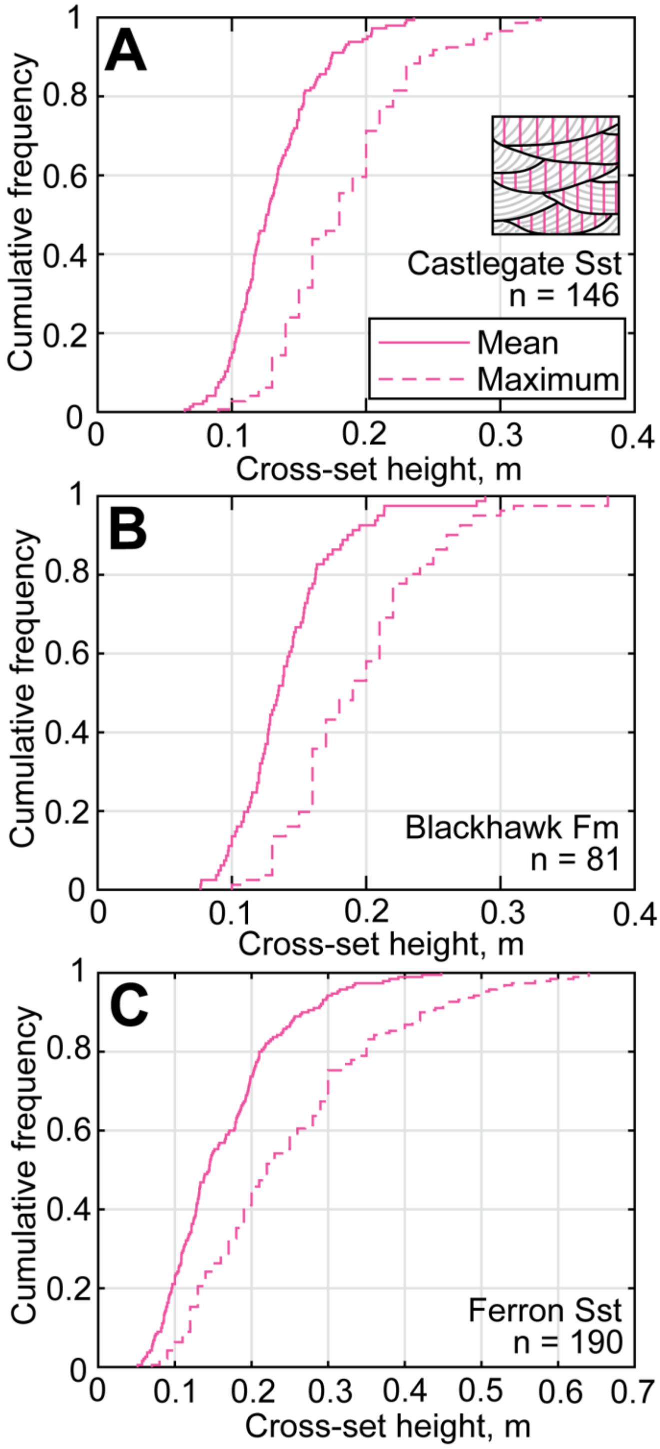

Figure 4: The cumulative frequency of the mean, median and maximum cross-set height for (A) the Castlegate Sandstone, (B) the Blackhawk Formation, and (C) the Ferron Sandstone. The solid pink line indicates the measured mean and the dashed pink line indicates the measured maximum. n indicates the number of cross-sets in which height distributions were measured, and therefore the number of cross-sets from which a mean and maximum were subsequently extracted. The inset in A is a schematic representation of how height distributions were measured within each cross-set.

[1 column figure]

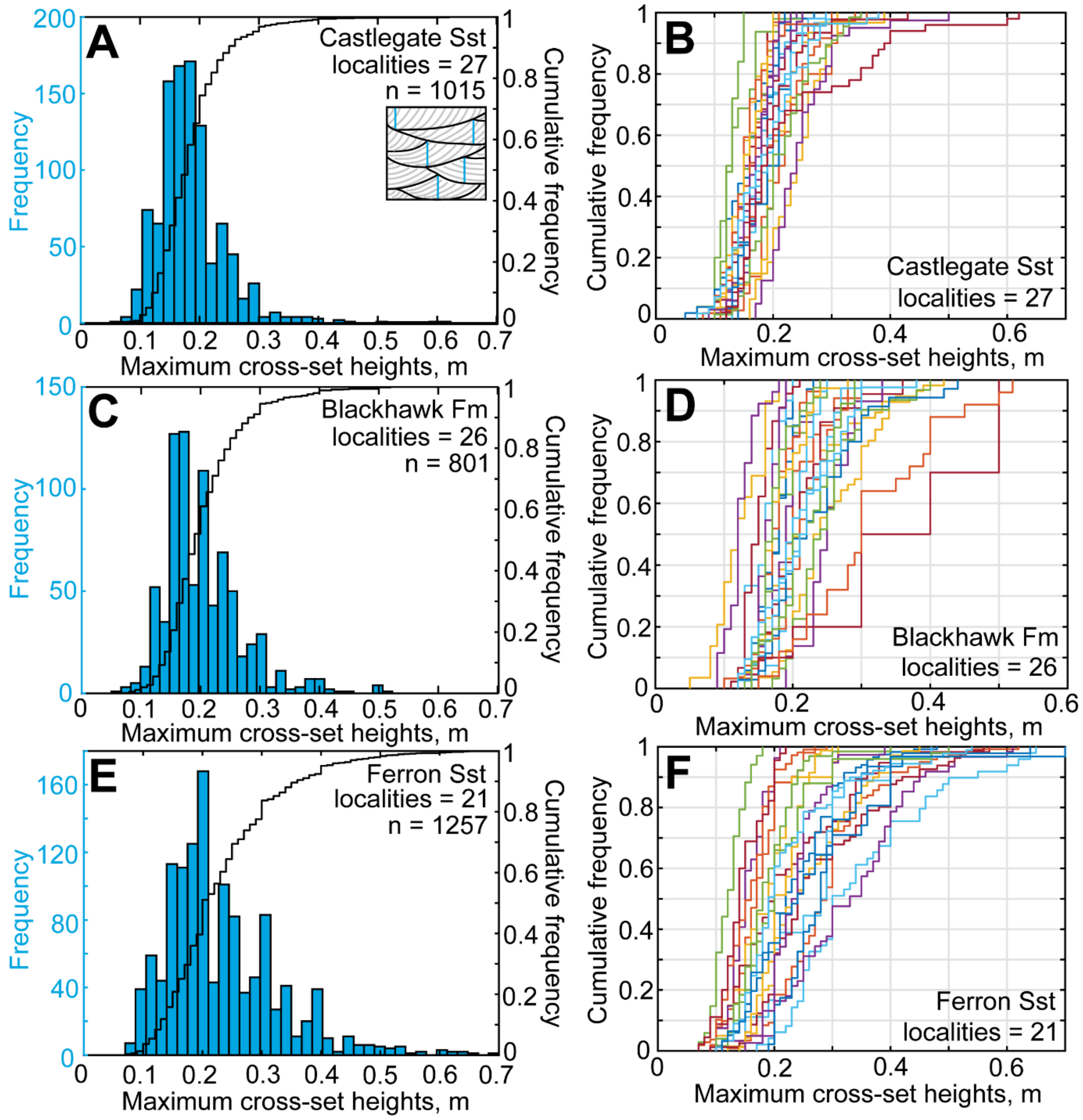

Figure 5: A) The frequency (left y axis; blue) and cumulative frequency (right y axis; black) of maximum cross-set heights measured across the Castlegate Sandstone. n indicates the total number of cross-sets measured for the entire formation, and the number of localities refers to the field sites across which these measurements were made. Measurements at each locality were for a population of related cross-sets within cosets, and typically comprised ~25–75 measurements. B) The cumulative frequency of maximum cross-set heights for each locality within the Castlegate Sandstone. C) The frequency and cumulative frequency of maximum cross-set heights measured across the Blackhawk Formation. D) The cumulative frequency of maximum cross-set heights for each locality within the Blackhawk Formation. E) The frequency and cumulative frequency of maximum cross-set heights measured across the Ferron Sandstone. F) The cumulative frequency of maximum cross-set heights for each locality within the Ferron Sandstone. The inset in A is a schematic representation of how maximum heights were measured across populations of cross-sets.

[1.5 or 2 column figure]

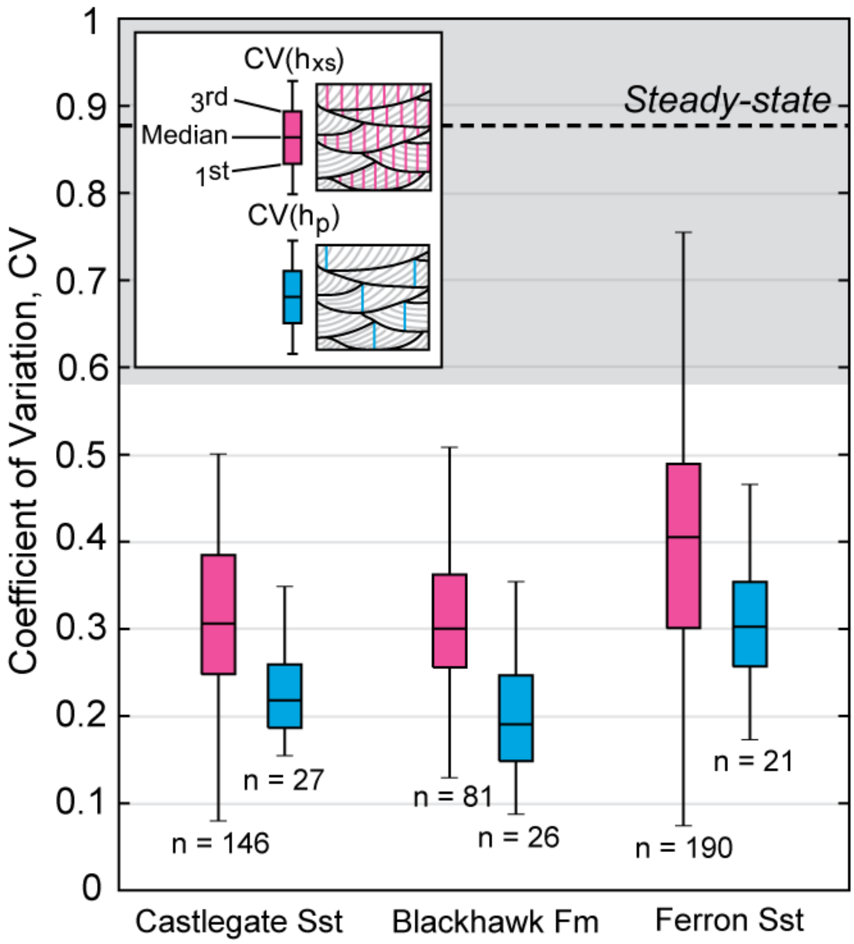

Figure 6: The coefficient of variation, *CV*, of cross-set heights measured in the Castlegate Sandstone, Blackhawk Formation, and Ferron Sandstone. Pink boxes indicate *CV*s of height distributions within individually measured cross-sets ($CV(h_{xs})$, with n indicating the number of individually measured cross-sets. The blue boxes indicate *CV*s of height distributions across a population of (related) cross-sets ($CV(h_p)$, with n indicating the number of field localities at which a population of cross-set heights was measured. At each locality, the population of measured cross-sets typically included ~25–75 cross-sets. Insets within the key demonstrate, schematically, how heights would have been measured for both $CV(h_{xs})$ and $CV(h_p)$ respectively (see Methods). The central mark of each box indicates the median estimate, and the bottom and top edges of each box indicate the 1st and 3rd quartiles (or 25th and 75th percentiles), respectively. The whiskers extend to the most extreme values of *CV* that are not considered to be outliers. The dashed black line indicates the theoretical steady-state *CV* of 0.88, following Paola and Borgman (1991), and the grey shaded region indicates the empirical steady-state *CV* of 0.88±0.30, following Bridge (1997).

[1.5 column figure]

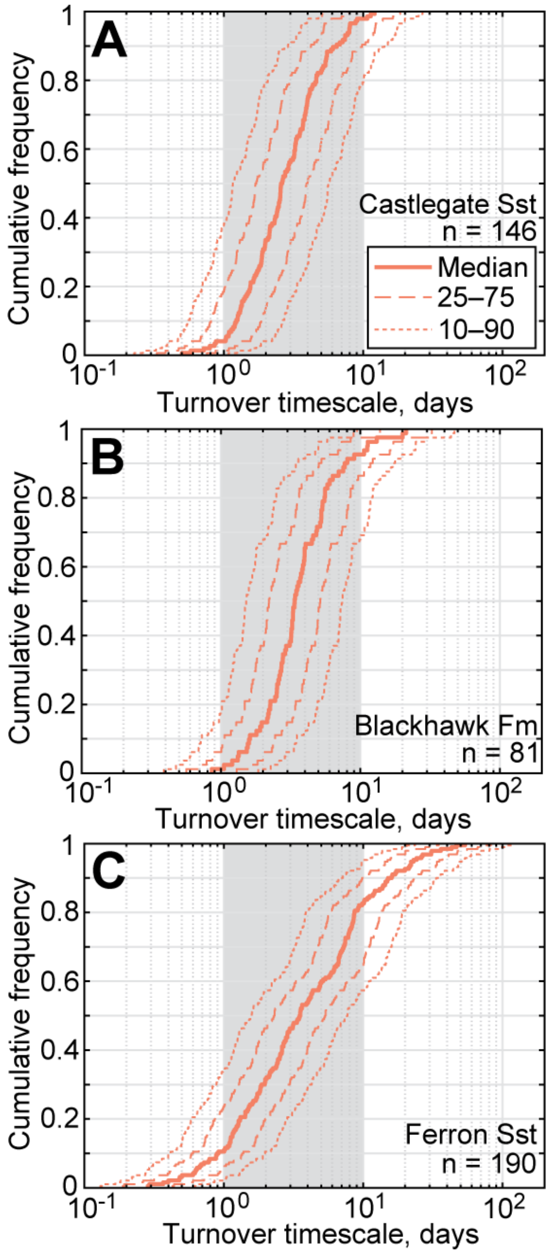

Figure 7: The cumulative frequency of estimated turnover timescales, T_t, calculated for (A) the Castlegate Sandstone, (B) the Blackhawk Formation, and (C) the Ferron Sandstone (see Supplementary Material). T_t was calculated for each cross-set from which a cross-set height distribution was measured, using the mean height and the measured grain-size (Fig. 3; see Methods). n indicates the number of T_t values that were calculated (equal to the number of measured cross-set height distributions). The solid orange line indicates the median T_t, the dashed orange lines indicate the 25^{th}–75^{th} percentile range of T_t values, and the dotted orange lines indicate the 10^{th}–90^{th} percentile range of T_t values, which we offer as a plausible spread of values for the mean (see Supplementary Methods). Grey shaded region indicates T_t values of 1–10 days; for the Castlegate Sandstone and Blackhawk Formation, ~90–95% of median T_t values fall within this range and, for the Ferron Sandstone, ~70% of median T_t values fall within this range.

[1 column figure]

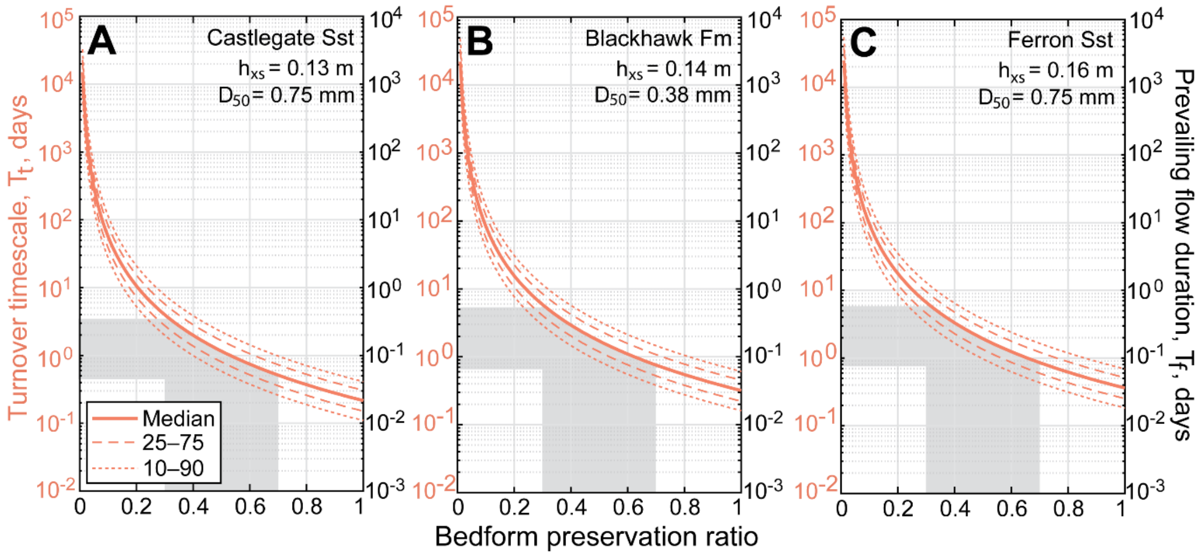

Figure 8: Turnover timescales, T_t, reconstructed for the Castlegate Sandstone, Blackhawk Formation and Ferron Sandstone using a range of preservation ratios. For these purposes, the mean cross-set height (h_{xs}) and median grain-size (D_{50}) for each geologic formation have been used (i.e. the mean and median across all measured cross-set distributions). The solid orange line indicates the median T_t, the dashed orange lines indicate the 25th–75th percentile range of T_t values, and the dotted orange lines indicate the 10th–90th percentile range of T_t values, which we offer as a plausible spread of values for the mean (see Supplementary Methods). The grey region highlights the range of median T_t values associated with a plausible range of bedform preservation ratios; steady-state bedform preservation ratios are ~0.3, and Leary and Ganti (2020) documented that higher bedform preservation ratios may extend up to ~0.7 during flash floods. On the right y axis, we show reconstructed prevailing flow durations, T_f, for the scenario in which T_f is a factor of 10 smaller than the reconstructed bedform turnover timescale.

[2 column figure]

Supplement to *Field evidence for disequilibrium dynamics in preserved fluvial cross-strata: A record of discharge variability or morphodynamic hierarchy?*

Sinéad J. Lyster[1], Alexander C. Whittaker[1], Elizabeth A. Hajek[2] and Vamsi Ganti[3,4]*

[1]Department of Earth Science and Engineering, Imperial College London, London, UK.
[2]Department of Geosciences, The Pennsylvania State University, Pennsylvania, USA.
[3]Department of Geography, University of California Santa Barbara, California, USA.
[4]Department of Earth Science, University of California Santa Barbara, California, USA.
**s.lyster17@imperial.ac.uk*

Contents:

S1. Field localities

Table S1: *Field localities visited in this study. Localities are grouped by field area (e.g., Price Canyon, Wattis Road; see Figure 1 in main text) and subdivided by formation (i.e., Blackhawk Formation, Castlegate Sandstone and Ferron Sandstone).*

Location and stratigraphic interval		**Field sites**	**Elevation, m (±3–4)**
Last Chance Creek	Ferron Sandstone	N38 40 18.9, W111 24 52.5	2255
		N38 40 20, W111 24 45.3	2241
		N38 40 21.7, W111 24 17.1	2218
		N38 40 17.5, W111 24 12	2209
		N38 40 12, W111 24 2.5	2190
		N38 40 7.7, W111 23 50.3	2179
		N38 40 9.1, W111 23 44.8	2187
		N38 40 8.9, W111 23 53.6	2215

Link Canyon	Blackhawk Formation	N38 57 42.1, W111 19 57.4	2363
		N38 57 39.7, W111 19 53.9	2383
		N38 57 41.4, W111 19 53.0	2398
		N38 57 44.3, W111 19 53.8	2421
		N38 57 48.4, W111 19 53.9	2473
		N38 57 58.3, W111 19 57.3	2538
		N38 57 52.8, W111 19 55.8	2509
		N38 57 51.4, W111 19 55.0	2500
	Castlegate Sandstone	N38 58 05.9, W111 19 56.6	2572
		N38 58 08.0, W111 19 55.8	2584
		N38 58 10.6, W111 19 54.2	2600
Price Canyon	Blackhawk Formation	N39 44 11.0, W110 50 47.7	1932
		N39 44 08.4, W110 50 46.9	1947
	Castlegate Sandstone	N39 45 05.1, W110 53 10.3	1920
		N39 44 48.5, W110 49 58.1	1969
		N39 44 52.6, W110 49 55.4	1983
		N39 45 01.3, W110 49 43.5	2000
		N39 45 03.0, W110 49 40.6	1999
		N39 45 10.5, W110 49 35.8	2008
		N39 45 12.0, W110 49 34.8	2003
Salina Canyon	Blackhawk Formation	N38 54 00.8, W111 39 53.8	1861
		N38 53 51.5, W111 39 02.3	1885
		N38 54 29.6, W111 41 46.8	1802
		N38 54 13.8, W111 39 05.9	1926
	Castlegate Sandstone	N38 54 52.9, W111 38 06.5	2036
		N38 54 52.3, W111 38 08.7	2017
		N38 54 50.6, W111 38 18.1	2009
		N38 54 52.6, W111 38 20.2	2030
		N38 54 53.7, W111 38~20.2	2035
		N38 54 33.0, W111 42 32.7	1779
		N38 54 57.1, W111 38 20.3	2076

		N38 54 59.4, W111 38 13.1	2111
Straight Canyon	Blackhawk Formation	N39 16 56.6, W111 13 58.0	2027
		N39 16 46.2, W111 13 41.9	2010
		N39 16 29.1, W111 13 11.9	1996
		N39 17 16.2, W111 14 37.5	2047
		N39 17 15.7, W111 14 30.4	2043
		N39 17 05.7, W111 14 10.5	2037
		N39 17 36.5, W111 16 16.7	2146
		N39 17 19.3, W111 16 00.0	2129
		N39 17 20.9, W111 15 19.8	2102
	Castlegate Sandstone	N39 17 51.9, W111 16 18.0	2161
		N39 18 28.6, W111 16 13.2	2181
		N39 18 55.2, W111 16 06.2	2238
Wattis Road	Blackhawk Formation	N39 31 45.5, W111 02 16.0	2577
		N39 31 11.9, W111 01 56.9	2692
		N39 31 19.8, W111 01 58.4	2655
		N39 31 20.7, W111 02 37.2	2798
		N39 31 14.3, W111 02 13.8	2765
	Castlegate Sandstone	N39 31 28.6, W111 02 44.9	2844
		N39 31 31.7, W111 02 50.6	2877
		N39 31 30.2, W111 02 46.4	2861
		N39 31 33.5, W111 02 53.2	2889
Willow Basin	Ferron Sandstone	N38 34 50.9, W111 28 6.2	2668
		N38 34 49, W111 28 6.5	2636
		N38 34 48.9, W111 28 4.5	2631
		N38 34 47.6, W111 28 5.4	2592
		N38 34 35.1, W111 27 48.4	2537
Willow Creek	Ferron Sandstone	N38 44 0.4, W111 18 47.2	1965
		N38 43 37.4, W111 18 46.5	1926
		N38 43 25.2, W111 18 45.9	1895

S2. Extended methodology: Estimation of bedform turnover timescale

As detailed in the main text, we reconstructed bedform turnover timescales, T_t, i.e., the time taken to displace the volume of sediment of the bedform (per unit width), following Martin and Jerolmack (2013) and Myrow et al. (2018), as:

$$T_t = \frac{\lambda h_d \beta}{q_b}, \qquad \text{[Eq. S1]}$$

where λ is bedform wavelength, h_d is the mean original bedform (i.e., dune) height, β ~0.55 is the bedform shape factor and q_b is the unit bedload flux. To use this framework, we first reconstructed h_d as a function of mean cross-set height, h_{xs}, using the relation of Leclair and Bridge (2001),

$$h_d = 2.9(\pm 0.7)h_{xs}, \qquad \text{[Eq. S2]}$$

where 2.9 is the mean (μ) and 0.7 is the standard deviation (σ). The above relation was experimentally derived for steady-state conditions, i.e., bedform preservation ratio (h_{xs}/h_d) of ~0.3. However, bedform preservation in disequilibrium conditions may imply that h_{xs}/h_d is higher (Jerolmack & Mohrig, 2005; Reesink et al., 2015; Ganti et al., 2020; Leary & Ganti, 2020). Initially, we assumed h_{xs}/h_d of ~0.3, which means that T_t estimates are maximum values. We subsequently evaluated the sensitivity of T_t to h_{xs}/h_d (see Methods in main text). Finally, we estimated likely values of h_{xs}/h_d for each geologic formation using available data (Section S3), which broadly range from 0.3–0.7, and used these values to contextualise the implications of this sensitivity on our results (Figure 8 in main text).

We used a Monte Carlo uncertainty propagation method to estimate uncertainty (c.f. Lyster et al., 2021). In doing so, we offer plausible spreads of values for the median of each reconstructed parameter. From Equation S2, we generated 10^6 random samples of the model parameter between bounds defined by μ−σ and μ+σ. To avoid introduction of additional assumptions, we generated these samples from a uniform distribution as the shape and the scale of the full distribution of the data is unknown. These 10^6 samples were used to calculate 10^6 values of h_d, and these results were propagated through subsequent calculations. Given that Equation S2 assumes steady-state flow conditions and a h_{xs}/h_d value of ~0.3, and that we randomly sampled the model parameter between μ−σ and μ+σ, we note that our uncertainty analysis analytically accounts for some variability in h_{xs}/h_d, between ~0.28 and ~0.45.

To reconstruct formative flow depth, H, we used the bedform height−flow depth scaling relation of Bradley and Venditti (2017), which was derived using >380 empirical data. Bradley and Venditti (2017) presented a non-parametric relation which characterized their data, which did not assume an underlying distribution for the scaling parameter. In this relation, median H is given as

$$H = 6.7h_d, \qquad \text{[Eq. S3]}$$

with a probabilistic uncertainty estimator in which the 1st and 3rd quartiles of H are given by H=4.4h_d and H=10.1h_d, respectively (Bradley & Venditti, 2017). We generated 10^6 random samples between 4.4 and 10.1, again from a uniform distribution, and reconstructed 10^6 values of H in these ancient fluvial systems using Equation S3. These values were then used to estimate bedform wavelength, λ, as λ=7.3H, following van Rijn (1984).

To reconstruct palaeoslope, we used the empirical method of Trampush et al. (2014). Palaeoslopes may also be calculated by a Shields stress inversion where the dimensionless Shields stress is known (or where it can be estimated using, e.g., bedform stability diagrams (Carling, 1999)). However, we implemented the method of Trampush et al. (2014) for consistency with the method that Mahon and McElroy (2018) used to derive Equations S5 and S6. In addition, previous studies have shown that both palaeoslope methods recover similar values for sand-grade grain-sizes (Ganti et al., 2019; Lyster et al., 2021). Trampush et al. (2014) expressed palaeoslope, S, as

$$\log S = \alpha_0 + \alpha_1 \log D_{50} + a_2 \log H, \qquad \text{[Eq. S4]}$$

where $\alpha_0 = -2.08 \pm 0.036$, $\alpha_1 = 0.254 \pm 0.016$, and $\alpha_2 = -1.09 \pm 0.044$ are constants. We randomly sampled 10^6 values of α_0, α_1, and α_2 (uniformly distributed between $\mu-\sigma$ and $\mu+\sigma$) and reconstructed 10^6 values of S.

To calculate characteristic bedform migration velocity, V_c, and therefore unit bedload flux, q_b, we used the bedform-scale (as opposed to grain-scale) approach of Mahon and McElroy (2018), in which q_b is estimated geometrically, per unit width, as a function of bedform migration velocity, V_c. These variables are given as:

$$\log V_c = \beta_0 + \beta_1 \log S, \qquad \text{[Eq. S5]}$$

$$q_b = (1-\varphi)\frac{h_d V_c}{2}, \qquad \text{[Eq. S6]}$$

where $\beta_0 = 0.6113 \pm 0.144$ and $\beta_1 = 1.305 \pm 0.0515$ are constants, and φ is a dimensionless bed porosity of 0.5 (Mahon & McElroy, 2018). To reconstruct V_c, we randomly sampled 10^6 values for the model parameters, β_0 and β_1, from a uniform distribution between bounds defined by $\mu-\sigma$ and $\mu+\sigma$. These values were then used to estimate q_b (Equation S6).

Having calculated 10^6 values of h_d, H, λ, S, V_c, and q_b, we reconstructed T_t using Equation S1. This recovered 10^6 values of T_t in units of seconds which we converted to days. From these values, we extracted median T_t, the 25–75 percentile range of T_t (or the 1st–3rd interquartile range of T_t), and the 10–90 percentile range of T_t. Given that the errors and uncertainties associated with Equations S2–S6 are propagated through the methodology, and that these errors and uncertainties are compounded on top of each other, we suggest that the 10–90 percentile range of T_t offers plausible minimum and maximum values for median T_t, with the 25–75 percentile range of T_t highlighting where true values of median T_t are most likely to occur between these bounds.

S3. Constraints on bedform preservation ratios

As discussed in the main text, and above, the scaling relation of Leclair and Bridge (2001) (Equation S2) is derived for steady-state conditions, which implies that reconstructed H values are also steady-state estimates. However, it is expected that h_{xs}/h_d is higher in disequilibrium conditions (see main text). The ability to constrain h_{xs}/h_d from geological outcrop would be useful for evaluating the nature of bedform preservation, however this is difficult in practice.

In order to accurately constrain h_{xs}/h_d, we ideally require systematic measurements of cross-set heights and knowledge of their original bedform heights, however it is not possible to know original bedform heights in ancient fluvial systems. Instead, we can contrast cross-set heights with independent proxies of H, e.g., barform heights. If H values reconstructed from mean cross-set heights using steady-state assumptions agree with independent proxies of H, then this might imply that h_{xs}/h_d was truly ~0.3. However, this approach requires us to assume the relationship between the original bedform height and the palaeoflow depth (Equation S3) in order to recover a value for h_{xs}/h_d. Reconstructions of h_{xs}/h_d are therefore estimates. Moreover, barform heights are a proxy for maximum palaeoflow depths which, given the possibility that mean palaeoflow depths are smaller, will act to decrease the estimated value of h_{xs}/h_d. This is particularly true where the heights of point bar deposits are used as independent proxies of H, as flow depths in meandering systems are typically greater on meander bends. One further issue with this approach is that the barforms themselves may not be fully preserved (Chamberlin & Hajek, 2019).

In this study, despite our detailed data collection, we do not have the desired spatiotemporal resolution of field measurements to accurately constrain h_{xs}/h_d., i.e., we do not have a mean cross-set height and the mean height of the associated barform for each measured cross-set. However, as a starting point, we compared mean cross-set heights across our field areas (Fig. 1 in main text) with mean barform heights in published literature. Based on stratigraphic observations, detailed below, we predict that values of h_{xs}/h_d likely ranged between 0.3 and 0.7. This suggests that uncertainty margins in Equation S2, which analytically account for variability in h_{xs}/h_d between ~0.28 and ~0.45, are reasonable. It is unlikely that h_{xs}/h_d is much smaller than ~0.3 because, as mentioned in the main text, if h_{xs}/h_d is much smaller than ~0.3 then T_t rapidly increases from 10^1 to 10^5 days (Eq. S2 and S3), which are implausible bedform migration timescales.

We recovered median values of ~0.13–0.14 m for the Blackhawk Formation and Castlegate Sandstone, but which broadly span 0.1–0.2 m. H values reconstructed using steady-state assumptions have previously been verified for the Blackhawk Formation and Castlegate Sandstone by Lyster et al. (2021). The authors reconstructed median H values of 2–4 m from cross-sets spanning the Blackhawk Formation and Castlegate Sandstone at localities along the eastern front of the Wasatch Plateau (Lyster et al., 2021). These H values are in broad agreement with H values independently inferred from bar-scale clinoform heights, which have means of ~3–3.5 m, but which typically span 1–8 m (Adams & Bhattacharya, 2005; Lynds & Hajek, 2006; McLaurin & Steel, 2007; Hajek & Heller, 2012; Chamberlin & Hajek, 2019; Lyster et al., 2021). Assuming the model parameter in Equation S3 is true, we might expect values of h_{xs}/h_d up to 0.6–0.7.

Meanwhile, for the Ferron Sandstone, H values reconstructed using steady-state assumptions have not previously been verified. Here, from individually measured cross-sets (n=190), we recovered median values of 0.15 m for mean cross-set heights, which broadly span 0.1–0.3 m. Using Equation S3 we project median values for H of ~3 m, but which broadly span 1–10 m (Equation S3). Independent proxies of H are limited for the Ferron Sandstone. As such, in the field we obtained new measurements of independent H proxies, e.g., laterally accreted point bar deposit heights, which we made using a Haglof Laser Geo laser range finder to a precision of ±5 cm, and which we used to supplement limited secondary data (Table S2). In the Ferron Sandstone, previous work has documented channel-fill deposits and laterally accreted point bars with heights of order 8–9 m (Cotter, 1971; Gardner et al., 2004; Garrison & Bergh, 2004). Here we report a broader range of heights for independent H proxies (Table S2). Across 35 measurements of point bar/lateral accretion set heights (Table S2), we recover a mean height of 4.7 m, with a 1^{st}–3^{rd} interquartile range spanning 2.9–6.5 m. Minimum and maximum heights are 1.1 and 10 m, respectively (Table S2). Similarly, if we assume the model parameter in Equation S3 is true, then we might expect h_{xs}/h_d values up to 0.6–0.7.

Table S2: *Independent measurements of palaeoflow depth indicators in the Ferron Sandstone*

Palaeoflow depth proxy	Height (m)	Source
Laterally accreted point bar deposit	9.1 (which was considered to represent meander bend flow depths — true flow depths were projected to be ~7.6)	Cotter (1971)
Laterally accreted point bar deposit	<8	Gardner et al. (2004)
Maximum thickness of channel-fill deposits	~9	Gardner et al. (2004)
Maximum thickness of channel-fill deposits	~9	Garrison and Bergh (2004)
Laterally accreted point bar deposits	8, 7.5, 9, 3.2, 4.8, 3.6, 6.5, 7.5, 3.6, 4.1, 2.7, 6.4, 5.5, 2.8, 1.1, 1.9, 7.5, 2.7, 7.1, 1.2, 4.4, 3.7, 3.1, 3.4, 3, 2.5, 5.9, 2.5, 4.7, 10, 4.2, 1.6, 3, 6.5, 10	**This study**
Maximum thickness of single channel storeys	8.6, 11.1, 12.2, 9, 7.6, 7.1, 3.9, 5.6, 2.6, 7.3, 12, 9.3	**This study**

S4. Data tables

We provide a Microsoft Excel spreadsheet containing field results and a selection of reconstructed palaeohydrologic parameters for the Blackhawk Formation, Castlegate Sandstone and Ferron Sandstone. Field data and results are reported per field area (see Fig. 1 in main text).

Adams, M. M., & Bhattacharya, J. P. (2005). No change in fluvial style across a sequence boundary, Cretaceous Blackhawk and Castlegate formations of central Utah, U.S.A. *Journal of Sedimentary Research, 75*(6), 1038-1051. doi:10.2110/jsr.2005.080

Bradley, R. W., & Venditti, J. G. (2017). Reevaluating dune scaling relations. *Earth-Science Reviews, 165*, 356-376. doi:10.1016/j.earscirev.2016.11.004

Carling, P. A. (1999). Subaqueous gravel dunes. *Journal of Sedimentary Research, 69*(3), 534-545. doi:10.2110/jsr.69.534

Chamberlin, E. P., & Hajek, E. A. (2019). Using bar preservation to constrain reworking in channel-dominated fluvial stratigraphy. *Geology, 47*(6), 531-534. doi:10.1130/G46046.1

Cotter, E. (1971). Paleoflow characteristics of a late Cretaceous river in Utah from analysis of sedimentary structures in the Ferron sandstone. *Journal of Sedimentary Research, 41*, 129–138. doi:10.1306/74D72202-2B21-11D7-8648000102C1865D

Ganti, V., Hajek, E. A., Leary, K., Straub, K. M., & Paola, C. (2020). Morphodynamic hierarchy and the fabric of the sedimentary record. *Geophysical Research Letters, 47*(14), e2020GL087921. doi:10.1029/2020GL087921

Ganti, V., Whittaker, A., Lamb, M. P., & Fischer, W. W. (2019). Low-gradient, single-threaded rivers prior to greening of the continents. *Proceedings of the National Academy of Sciences, 116*(4), 11652-11657. doi:10.1073/pnas.1901642116

Gardner, M. H., Cross, T. A., & Levorsen, M. (2004). Stacking Patterns, Sediment Volume Partitioning, and Facies Differentiation in Shallow-Marine and Coastal-Plain Strata of the Cretaceous Ferron Sandstone, Utah. In T. C. Chidsey, Jr., R. D. Adams, & T. H. Morris (Eds.), Regional to Wellbore Analog for Fluvial-Deltaic Reservoir Modeling: The Ferron Sandstone of Utah (Vol. 50, pp. 0): American Association of Petroleum Geologists. doi:10.1306/St50983

Garrison, J. R., Jr., & Bergh, T. C. V. v. d. (2004). High-Resolution Depositional Sequence Stratigraphy of the Upper Ferron Sandstone Last Chance Delta: An Application of Coal-Zone Stratigraphy. In T. C. Chidsey, Jr., R. D. Adams, & T. H. Morris (Eds.), Regional to Wellbore Analog for Fluvial-Deltaic Reservoir Modeling: The Ferron Sandstone of Utah (Vol. 50, pp. 0): American Association of Petroleum Geologists. doi:10.1306/St50983

Hajek, E. A., & Heller, P. L. (2012). Flow-depth scaling in alluvial architecture and nonmarine sequence stratigraphy: Example from the Castlegate Sandstone, central Utah, U.S.A. *Journal of Sedimentary Research, 82*(2), 121-130. doi:10.2110/jsr.2012.8

Jerolmack, D. J., & Mohrig, D. (2005). Frozen dynamics of migrating bedforms. *Geology, 33*(1), 57-60. doi:10.1130/G20897.1

Leary, K. C. P., & Ganti, V. (2020). Preserved fluvial cross strata record bedform disequilibrium dynamics. *Geophysical Research Letters, 47*(2), e2019GL085910. doi:10.1029/2019GL085910

Leclair, S. F., & Bridge, J. S. (2001). Quantitative interpretation of sedimentary structures formed by river dunes. *Journal of Sedimentary Research, 71*(5), 713-716. doi:1527-1404/01/071-713/$03.00

Lynds, R., & Hajek, E. (2006). Conceptual model for predicting mudstone dimensions in sandy braided-river reservoirs. *AAPG Bulletin, 90*(8), 1273-1288. doi:10.1306/03080605051

Lyster, S. J., Whittaker, A. C., Hampson, G. J., Hajek, E. A., Allison, P. A., & Lathrop, B. A. (2021). Reconstructing the morphologies and hydrodynamics of ancient rivers from source to sink: Cretaceous Western Interior Basin, Utah, USA. *Sedimentology*. doi:10.1111/sed.12877

Mahon, R. C., & McElroy, B. (2018). Indirect estimation of bedload flux from modern sand-bed rivers and ancient fluvial strata. *Geology, 46*(7), 579-582. doi:10.1130/G40161.1

Martin, R. L., & Jerolmack, D. J. (2013). Origin of hysteresis in bed form response to unsteady flows. *Water Resources Research, 49*(3), 1314-1333. doi:10.1002/wrcr.20093

McLaurin, B. T., & Steel, R. J. (2007). Architecture and origin of an amalgamated fluvial sheet sand, lower Castlegate Formation, Book Cliffs, Utah. *Sedimentary Geology, 197*(3), 291-311. doi:10.1016/j.sedgeo.2006.10.005

Myrow, P. M., Jerolmack, D. J., & Perron, J. T. (2018). Bedform disequilibrium. *Journal of Sedimentary Research, 88*(9), 1096-1113. doi:10.2110/jsr.2018.55

Reesink, A. J. H., Van den Berg, J. H., Parsons, D. R., Amsler, M. L., Best, J. L., Hardy, R. J., . . . Szupiany, R. N. (2015). Extremes in dune preservation: Controls on the completeness of fluvial deposits. *Earth-Science Reviews, 150*, 652-665. doi:10.1016/j.earscirev.2015.09.008

Trampush, S. M., Huzurbazar, S., & McElroy, B. (2014). Empirical assessment of theory for bankfull characteristics of alluvial channels. *Water Resources Research, 50*(12), 9211-9220. doi:10.1002/2014WR015597

van Rijn, L. C. (1984). Sediment transport III: bedforms and alluvial roughness. *Journal of Hydraulic Engineering, 110*(12), 1733-1754. doi:10.1061/(ASCE)0733-9429(1984)110:12(1733)